POLITECNICO DI TORINO

Master's Degree in Energetic and Nuclear Engineering
A.a. 2025/2026
Sessione di laurea Marzo 2026

Politecnico di Torino

Master's Degree Thesis

Structural analysis and optimization of wind turbine blades for offshore applications

Supervisors:
Prof. Giovanni BRACCO
Dr. Massimo SIRIGU

Candidate:
Riccardo Cannata

March 2026

Abstract

This master's thesis focuses on the structural design, optimization, and techno-economic assessment of a 15 MW offshore wind turbine blade in the Mediterranean Sea condition. In the current energy context, the optimisation of renewable energy technologies is playing an important role, especially for technologies such as offshore wind power, which are constantly evolving. The work aims to do a structural analysis and aero-structural optimization of a wind turbine blade in different wind conditions and do a simplified techno-economic modelling to evaluate its performance in different wind and geographical scenarios.
After a briefly introduction to wind energy, the study begins with the definition of a reference 15 MW offshore wind turbine blade layout using Co-Blade. The refence configuration includes aerodynamic parameters and a composite structural architecture based on carbon spar caps, glass fiber reinforcement, shear webs, and foam core panels.
Firstly, a frozen load optimization is performed, i.e. only the structural variables are allowed to change, then starting with this result, an aero-structural optimization process is performed. The blade is first optimized at rated wind speed (10.6 m/s) using a Particle Swarm Optimization (PSO) algorithm implemented in MATLAB. The objective function is defined as the ration between structural blade cost and Annual Energy Production (Cost/AEP), with structural and geometric constraints that must be respected. The optimization leads to a structurally efficient blade that satisfies all constraints while reducing the cost-to-energy ratio. To validate the results obtained, a robustness analysis of the optimization was performed, i.e. five runs are executed to verify the consistency of results.
After obtaining the optimized blade at rated conditions, further analyses are conducted to determine the wind speed at which the blade achieves its most favorable techno-economic performance. By re-optimizing the blade for wind speed between 10 m/s and 16 m/s, it is shown that this approach, using PSO, isn't optimum due to strong increases of uncertainty making the results not reliable. Suggesting a different method, like the shell model for finite element.
Before the techno-economic analysis a simplified parametric study is performed by introducing a global thickness multiplier to the geometric variable, allowing evaluation of blade behavior under different wind speed while maintaining structural constraint. The final part of the thesis is dedicated to techno-economic analysis. Using cost data for offshore wind farms and a simplified cost model expressed as a function of installed power, the Cost of Energy (COE) is calculated for wind speeds between 8 m/s and 16 m/s in three distinct locations: Mediterranean Sea, North Sea, and Atlantic Ocean. The same analysis is done for two configurations of wind farms: the bigger with 60 turbines, the smaller with 20 turbines. The analysis highlights how wind conditions, installed capacity, and spatial density influence overall energy cost and identifies the most favorable combination of wind speed and location.

Summary

List of Figure

List of Table

1 Introduction

Driven by the global energy transition, renewable energy technologies are experiencing rapid and continuous development. Among them, wind power has assumed a significant role, emerging as one of the most significant contributors within the overall energy mix. The basic concept of wind energy conversion is simple: wind turbines capture the kinetic energy contained in moving air and transform it into electrical power. A turbine consists of a rotor with multiple blades, connected to a nacelle housing the drivetrain and the generator. As the wind sets the blades in motion, the rotor turns, transmitting mechanical energy to the generator, which then converts it into electrical energy.

Wind energy production can be divided into two categories: onshore and offshore. Onshore wind farms benefit from relatively low installation costs and proximity to consumers, which reduces distribution losses. However, they are often criticised for their impact on the landscape and for noise emissions, which limit public acceptance and restrict further expansion in densely populated regions. Offshore wind, by contrast, is more efficient. Turbines installed at sea exploit stronger and more stable wind resources, free by topographical features that can negatively affect production on land. The trade-off, however, lies in higher installation and maintenance costs, which can be aggravated by severe marine conditions.

This thesis focuses on offshore wind energy, with particular attention to turbines in the 5–15 MW range and the significant costs associated with their installation. In recent years, global projects have increasingly been developed in deeper waters and farther from shore, in regions such as the coastlines of California, Japan, and Europe. These projects often require floating offshore wind turbines, highlighting how technological progress is enabling the industry to overcome the challenges imposed by site conditions.

The offshore technology is divided in fixed bottom and floating, considering the sea depth, lower for the first one, over 50 m for the second one.

For fixed-bottom offshore wind farms, monopiles remain the predominant substructure solution. Nevertheless, alternative foundations such as jackets and gravity-based systems are being adopted in locations with different soil and seabed characteristics. The choice of substructure depends on local environmental conditions, particularly water depth and seabed composition. For instance, significant differences can be observed between Northern Europe and the Mediterranean. In Northern Europe, where water depths are relatively shallow, fixed-bottom technology dominates. On the contrary, in the Mediterranean, the greater depths necessitate the adoption of floating wind technology.

These regional differences also lead to substantial variations in costs. Offshore wind projects in the Mediterranean face higher installation expenses compared to their

Northern European counterparts. This is reflected in the Levelized Cost of Energy (LCOE). Current estimates place the lowest LCOE in the Mediterranean at around 95 €/MWh, with projections suggesting a decrease to approximately 70 €/MWh by 2050. In Northern Europe, the LCOE is already significantly lower, averaging around 70 €/MWh, and forecasts indicate that it could fall below 50 €/MWh in the coming decades.

In summary, while offshore wind energy presents considerable economic and technological challenges, it also offers immense potential. Its continued development will be essential to meet global decarbonisation goals, particularly as innovations in turbine design, substructures, and floating technology progressively reduce costs and expand the geographical feasibility of offshore projects.

2 History

Wind power is a reliable source of clean energy that is growing worldwide, following the journey towards net zero.
The power of wind has been used throughout history, starting with sails for transport along rivers, then windmills and wind pumps for food production around the 11th century.
The use of wind energy dates back more than a thousand years. Early windmills with vertical-axis blades were built in Persia and mainly used for grinding grain. Later, similar systems spread across Europe, particularly in the Netherlands, where horizontal-axis designs became more common and were primarily applied in agricultural activities. These early technologies laid the foundation for the development of modern wind turbines.

Figure 1: old wind technologies [1]

A turning point came in the 1970s due to the energy crisis in the US, which forced researchers and leaders to explore alternative energy options.
The world's first wind farm was installed in December 1980 in New Hampshire,

consisting of 20 turbines, each with a capacity of 30 kilowatts. Although the project did not achieve its desired objectives, it laid the foundations for the subsequent Mod 2 of 7.5 MW, which demonstrated the feasibility of using large turbines to produce significant amounts of energy. Other wind turbines with increasingly larger rotor diameters were installed during that decade.

In 1991, the Vindeby plant, the world's first offshore wind farm, began operating off the coast of Denmark. It consisted of eleven 450 kW turbines with a total capacity of 5 MW.

This was followed by increasingly large installations, resulting in higher energy production. In 2010 3 GW (offshore) worldwide installed, expanded to 28.3 GW in 2019. This shows an increased installation of almost 30% per year. [1]

This continuous increase in installation and development leads to the technologies that are known today. Offshore turbines are mainly bottom fixed. This design features a monopile foundation, i.e. a hollow steel tube driven into the seabed, or a jacket, a lattice structure with three or four legs, typically fixed to the seabed using pin piles or suction buckets. However, these systems have the limitation of only being usable at shallow depths (less than 55 m).

For greater depths, floating wind turbines are used. There are many different designs for this technology, including semi-submersible substructures that typically consist of three or four outer buoyant columns or other floating elements that are connected using platforms. They are ballasted to provide additional stability.

Another important design is the spar substructure that use ballast-stabilised design. The structure comprises a tall cylindrical form incorporating dense ballast in its lower part. This configuration lowers the center of gravity below the center of buoyancy, thereby generating a restoring, self-righting motion.

Others are tension leg platforms or barge substructures and others that offer the potential for significant mass reduction but often increase the complexity of design, which is not optimal. Anyway, there are continuous improvements in these technologies, which will lead to a gradual increase in wind power.

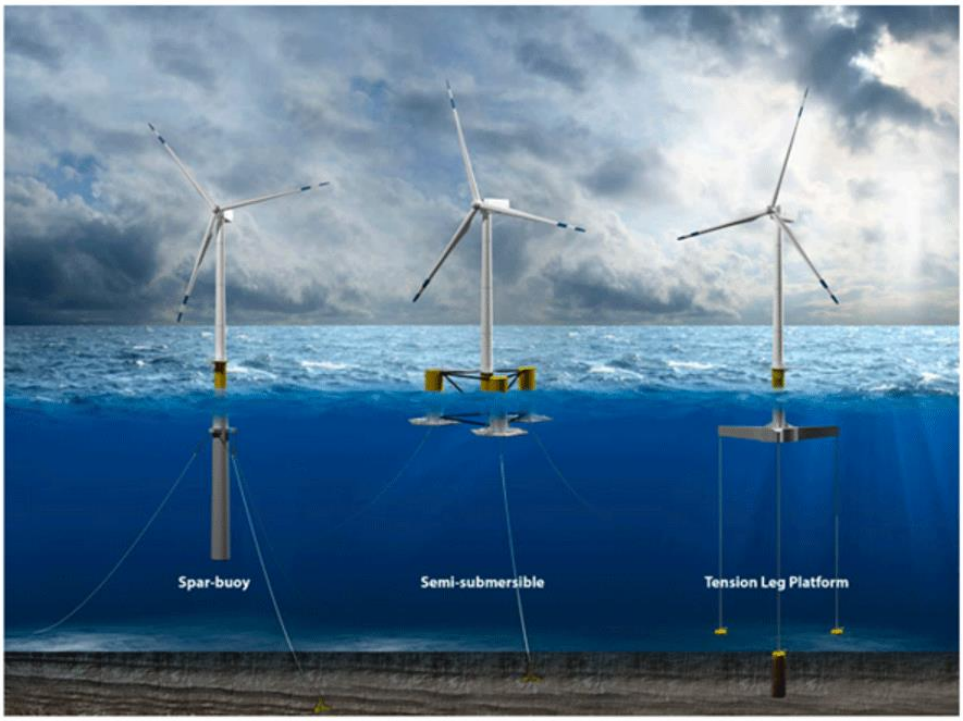

Figure 2: type of floating offshore wind turbine [2]

3 offshore wind turbine

3.1 Dimensions of wind turbine

The size of wind turbines has increased dramatically over the years to maximize energy production, since capturing more wind enables greater conversion into electricity. Early designs were relatively small, with rotor diameters of approximately 30 m, but steady growth in both blade length and tower height has led to today's record machines, which exceed 280 m in height and feature rotors spanning up to 230 m. The continuous increase in turbine size reflects the general tendency of the wind industry toward upscaling. From a theoretical point of view, the square–cube law indicates that the investment cost per installed megawatt is expected to grow with turbine size, since structural mass increases faster than the rated power output.
In practice, however, historical data show that ongoing technological progress has mitigated these scaling effects. Moreover, deploying larger offshore turbines reduces the number of units required to achieve a given wind farm capacity, lowering relative expenses related to foundations, installation, electrical interconnection, and offshore maintenance. Although the levelized cost of energy (LCOE) for offshore wind remains on average about twice that of onshore wind, it has declined significantly as turbine size has increased. Looking ahead, a key question for the sector is whether further upscaling can continue to reduce offshore LCOE or whether fundamental economic and practical limits will eventually be reached.

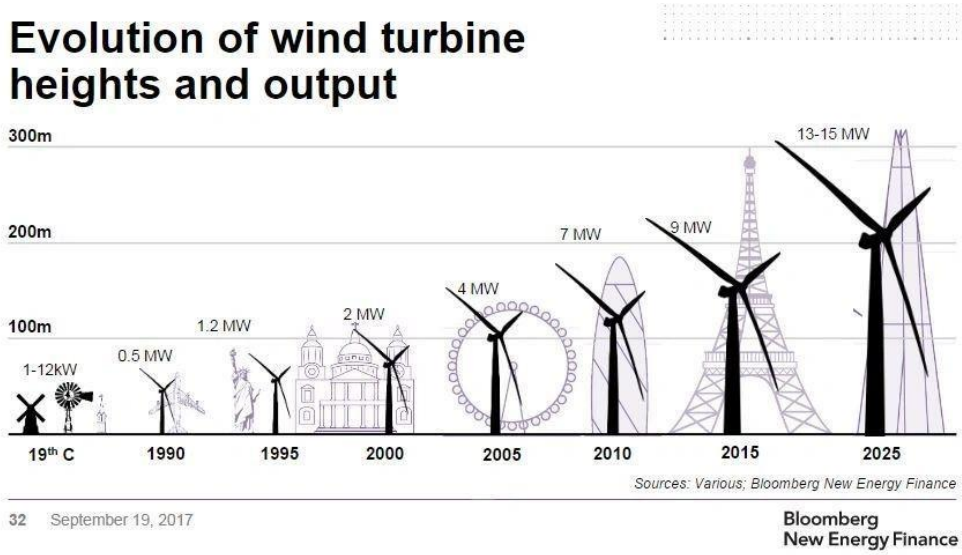

Figure 3: evolution of wind turbines [3]

To this increase in size follow a consideration of the external conditions, as they significantly influence structural loading, durability, and operational performance.

To ensure adequate safety and reliability, environmental and electrical parameters shall be explicitly incorporated into the design process and documented accordingly. Environmental conditions can be divided into two main categories: wind-related and other environmental factors. Electrical conditions refer to the characteristics of the power grid to which the turbine is connected.
External conditions are further classified as either normal or extreme. Normal external conditions represent recurrent load situations that occur throughout the turbine's operational life, whereas extreme conditions correspond to rare but potentially critical events. The design process must therefore account for combinations of these external conditions together with turbine operational modes and other relevant scenarios, forming the basis of the prescribed design load cases.
Wind conditions are the most influential external factor affecting the structural integrity of turbines. However, other environmental conditions must also be considered, as they can impact aspects such as control system performance, long-term durability, and resistance to corrosion.
The specific normal and extreme conditions to be applied in the design of wind turbines are shows in Table 1, in accordance with turbine classes:

Wind Class	I	II	III
V_{ref} (m/s)	50	42.5	37.5
V_{ave} (m/s)	10	8.5	7.5
$V_{ref,T}$ (m/s)	**57**		
A I_{ref}	0.16		
B I_{ref}	0.14		
C I_{ref}	0.12		

Table 1: wind classes [4]

- Vref is the reference wind speed average over 10 min.
- A designates the category for higher turbulence characteristics.
- B designates the category for medium turbulence characteristics.
- C designates the category for lower turbulence characteristics.
- Iref is the expected value of the turbulence intensity2 at 15 m/s.

The external conditions relevant for wind turbine design depend on the characteristics of the intended installation site or site type. To address this, wind turbine classes are defined based on reference wind speed and turbulence intensity parameters, with the aim of including most applications. These reference values are not intended to precisely describe a specific site, but rather to provide representative conditions applicable to a wide range of environments.
The classification system therefore establishes distinct levels of structural robustness,

each explicitly linked to wind speed and turbulence criteria. (The expression "turbulence" denotes random variations in the wind velocity from 10 min. averages).

3.2 Components of wind turbine

The turbine converts kinetic energy from the wind into three-phase AC electrical energy. Most designs have upwind, pitch controlled, variable speed rotors with three blades. Compared to onshore wind turbines, offshore turbines are larger and there is an increased focus on reliability and maintainability and a decreased focus on noise, visual and transport constraints. The design life of an offshore turbine is 25 years.
One component of the wind turbine is the nacelle, that supports the rotor and converts the rotational energy from the rotor into electrical energy. This includes the main bearing, gearbox (where used), generator, yaw bearing and yaw system. There are no major differences in the nacelles designed for floating or fixed offshore wind farms. Adjustments are needed to the control system to make the turbine suitable for application in floating.
There is a tower, typically a tubular steel structure that supports the nacelle, it also provides access to it, to house electrical and to control equipment. The hub height is about 135 m above sea level (depending on the rotor diameter).
Another crucial element is the rotor, which extracts kinetic energy from the air and convert this into rotational energy in the drive train (typically for a 15 MW turbine has a diameter of 224 m).
The rotor consists of blade system, bearing and pitch system.
Higher tip speeds typically lead to more efficient energy capture, and tip speeds offshore are higher than those used onshore, but these are limited by design to avoid blade leading edge erosion.
Each blade is mounted on a bearing connected to the central hub, allowing the pitch mechanism to regulate the blade angle for power control, load reduction, and safe turbine operation. Independent hydraulic or electric pitch systems ensure functionality and reliability, even in case of individual system failure.

3.3 Rotor

As mentioned, the rotor is the part where wind energy is converted into momentum. The power extracted from the wind is:

$$P = \frac{1}{2}\rho C_p A\, U^3$$

Where:

- ρ is the air density [$\frac{kg}{m^3}$],
- C_p is the Power Coefficient,
- A defined with the area of the rotor [m^2],

- U is the wind velocity [$\frac{m}{s}$].

From Betz theory $C_{p,max} = \frac{16}{27}$, this value is obtained from a study whit no wake losses, so, taking into consideration the rotating wake, the power coefficient must be smaller than that maximum value.

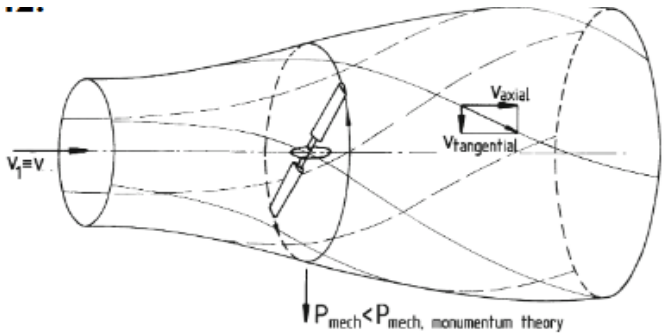

Figure 4: wind toward the rotor blade.

When exposed to airflow, bodies are subjected to two primary aerodynamic forces: drag, aligned with the flow direction, and lift, acting orthogonally. The attainable power coefficients differ depending on whether drag-based or lift-based mechanisms are used.
Today the most common rotor is aerodynamic lift based.

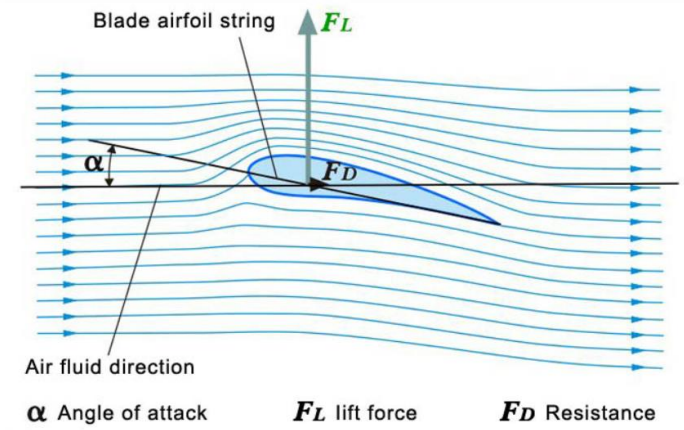

Figure 5: Attack angle of the airfoil normal operation.

The Figure 5 presents a cross-sectional airflow around a blade. The angle between the chord line and the flow direction is defined angle of attack α. During regular operation, airflow remains attached to the surface, producing higher velocity above than below, which result in lift (F_L) and drag (F_D) force.

This is the condition of large lifting force, and little drag force, but not always happen this situation.

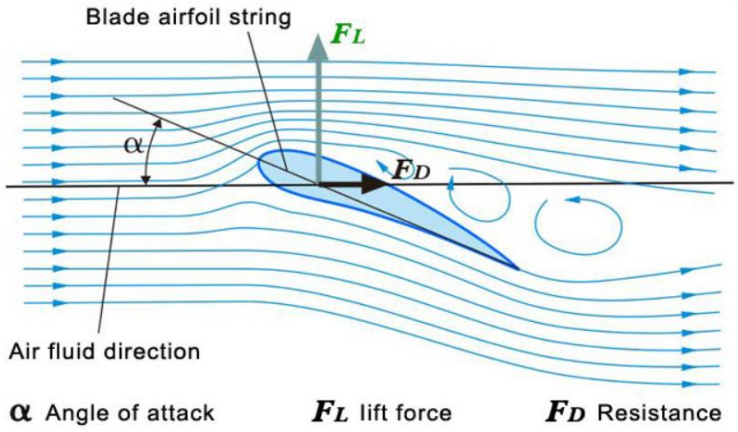

Figure 6: attack angle bigger than the critical one

At sufficiently large angle of attack α, airflow separation occurs above the airfoil, producing vortices near the leading edge. This leads to a rapid increase in drag and a simultaneous reduction in lift. This phenomenon is referred to as stall, and the corresponding threshold is defined stall or critical angle of attack.

3.3.1 Number of rotor blade

In today global market, the upwind, three bladed rotor is the most used configuration. The choice of the number of blades is a balance among blade stiffness, aerodynamic efficiency, and tower-shadow impulsive noise.
For efficiency considerations, in general, a high tip speed ratio λ is desirable since meaning in high rotational speed of the shaft, in fact:

$$\lambda = \frac{Tip\ speed\ of\ Blade}{Wind\ speed} = \frac{\Omega \cdot R}{V}$$

Where:

- Ω is the rotational speed of the rotor [rad/s],
- R is the radius of the rotor,
- V is the wind speed.

However, this can't be too high, so a typical value of the TSR for a three blades wind turbine is in the range 6-8.

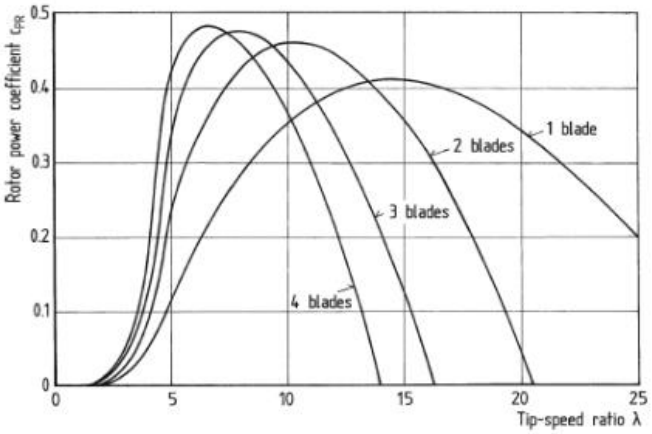

Figure 7: performance curve at different blades number.

For what concern the number of blades the performance curve is used to define the best solution, as already mentioned higher the power coefficient, higher the power output. As in Figure 7 increasing blade number reduces TSR corresponding at the maximum Cp and increase the Cp up to a certain point, but the shade effect of blades rise, decreasing the Cp.
Other considerations that favour three blades are the noise, considered less annoying respect to the two blades rotor, the more dynamically balanced rotor and the more beneficial rotor dynamics tend to result in lower operating and maintenance cost.

3.4 Load

Before analysing the shape of the blade, it is necessary to understand the loads to which it is subjected.
The type of load can be divided in:

- Steady load
- Cyclic load
- Transient load
- Stochastic load
- Resonance-induced loads

3.4.1 Steady load

These are the loads that do not vary over a relatively long time period. For example, a steady wind blowing on a stationary wind turbine is considered a static load on the tower, nacelle and foundation. Instead, the same steady wind blowing on a rotating wind turbine, induce a steady load on the blades.

3.4.2 Cyclic load

Cyclic loads are loads that change in a regular or periodic way over time. In wind

turbines, they mainly originate from variations in wind speed across the rotor plane while the blades are rotating. As a result, the aerodynamic conditions experienced by the rotor vary continuously. Cyclic loads can also arise from design features that break the symmetry of the rotor around its axis, leading to unsteady loading conditions. In addition, certain turbine operations, such as yaw motion, generate gyroscopic forces that may become significant, especially at high yaw rates.
Last source of cyclic load is the gravity, which introduce a load every time the rotor does a revolution.

Figure 8: Gravity load.

3.4.3Transient load

Transient load are sudden changes in the magnitude and/or the direction of a torque load in response to some temporary external event. Usually, the worst torsional vibrations or torque generally occur during transient events, such as emergency stops, load in the drive train resulting from the application of a brake (Figure 9) or also impulsive load due to wind gusts.

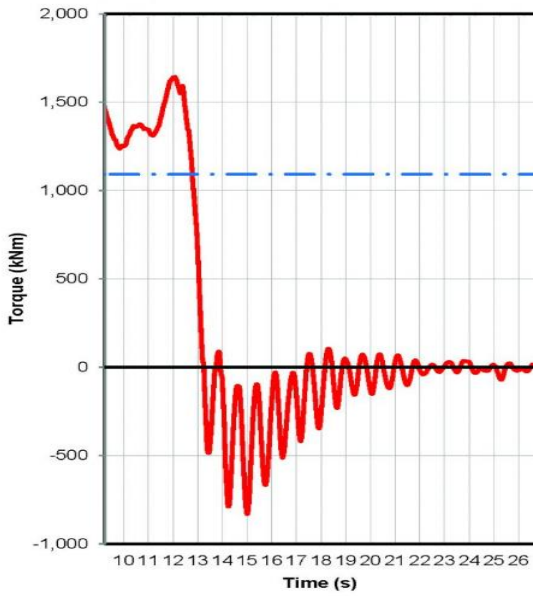

Figure 9: Transient load. [5]

Such conditions may induce significant vibration excitation. Each spike (observable in Figure 9) on the response curve indicates a torsional reversal, requiring energy dissipation and producing impact loads on the bearings distributed throughout the turbine.

3.4.1 Stochastic load

The stochastic load is a time varying load, in response to a random and fluctuation force applied by the wind, such as turbulence. In many cases the mean value may be relatively constant, but there may be significant fluctuations from that mean.

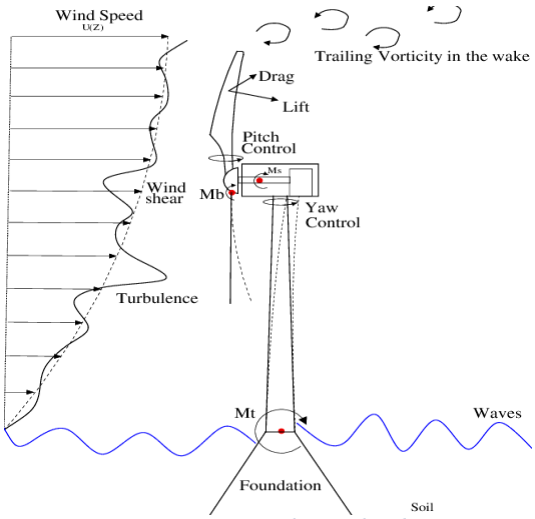

Figure 10: Stochastic load.

3.4.1 Resonance induced loads

The resonance induced loads are cyclic loads that result from the dynamic response of some part of the turbine being excites at one of its natural frequencies, for example from the excitation force on the nacelle and amplified due to the slim tower structure with a concentrated load on the top.
These loads must be avoided, they are mentioned separately because of their possibly serious consequences.

3.5 Blade description

The blade of a wind turbine involves several structural units, including the skin, spar caps, and web (Figure 11). The spar caps and web constitute the main spar, the principal load-bearing element, which determines stiffness, ultimate strength, and shear capacity. The skin, in turn, has limited structural function and primarily shapes the blade's aerodynamic profile.

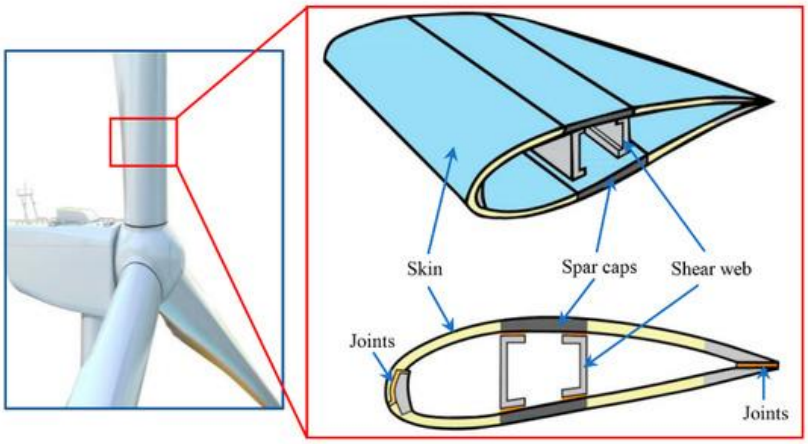

Figure 11: Blade's section. [6]

To guarantee structural strength, the blade thickness near the root must be important, while ensuring that aerodynamic resistance remains within acceptable limits. Consequently, turbine blades are required to achieve a high maximum lift coefficient, a large lift-to-drag ratio, stable aerodynamic behavior under stall conditions.

3.5.1 Blade structure

The objective of the blade structure is to get the airfoil to work at the angle of attack before stall to get maximum lift and less resistance. To obtain the most suitable angle of attack is properly selected the pitch angle β (the angle between the airfoil linear

velocity u and the cord line)

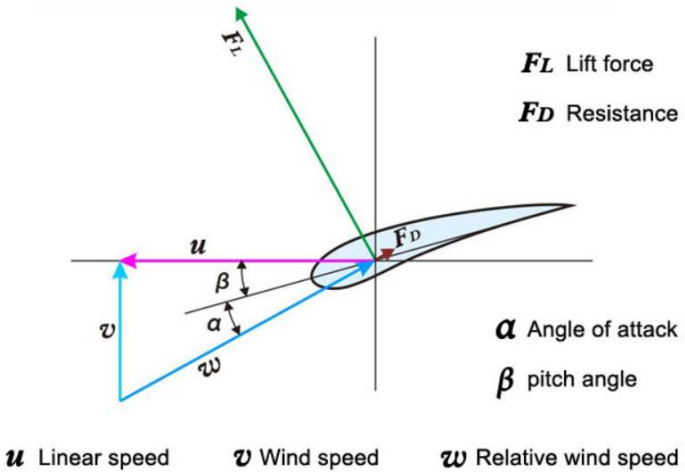

Figure 12: blade structure [7]

Due to rotation, the linear velocity "u" of a blade varies along the length of the blade, being maximal at the tip and minimal at the root. At constant wind speed v, this causes the inflow angle to be lowest at the tip and highest at the root. To achieve optimal angle of attack for all sections, the blade must be made torsional.

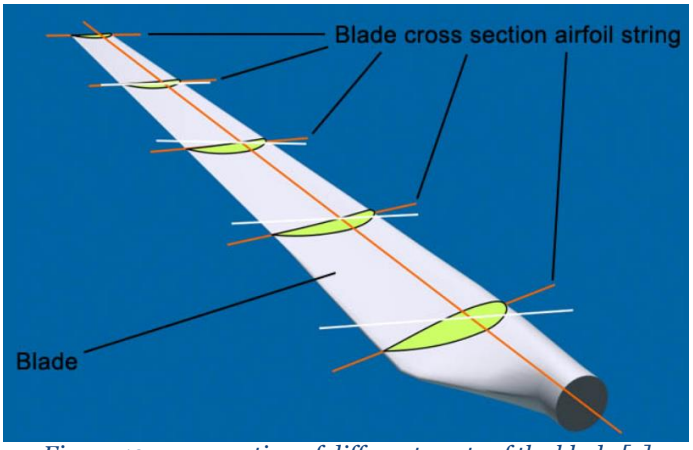

Figure 13: cross section of different parts of the blade [7]

From Figure 13, it can be seen that the angle between the cross-section strings and the horizontal plane change along the blade, and it is maximum at the root of the blade.

3.5.2 Blade material

The structural behaviour of a large wind-turbine blade is strongly influenced by the properties of the composite materials from which it is manufactured. These materials are distributed along the span and across the cross-section. Modern blades for multi-megawatt turbines rely almost entirely on fibre-reinforced polymer (FRP)

composites, chosen for their high specific stiffness, good fatigue resistance, and ability to withstand cyclic environmental loading. Because each blade region experiences different stresses and deformation demands, the material system is not uniform.
A typical blade can be divided into three principal material regions, each designed to fulfil a structural function (Figure 14):

- Spar caps (AA in the figure): Located along the suction and pressure sides, these longitudinal laminates carry the majority of the flapwise bending loads. To resist the large tension and compression forces generated during turbine operation, spar caps are almost exclusively made of unidirectional (UD) fibres aligned along the blade span. UD carbon or UD glass are used depending on stiffness and cost requirements. Carbon is preferred for very large offshore blades due to its high specific stiffness, which increases natural frequencies and reduces overall mass.
- Shear webs (BB in the figure): Webs are vertical internal panels connecting the two spar caps, forming a closed box-beam structure. Their main purpose is to provide torsional stiffness and shear load transfer between the caps. For this reason, they are typically manufactured using ±45° glass fibre or triaxial laminates, which offer high shear rigidity. Local UD reinforcements may also be added where shear and axial loads combine.
- Shell panels (outer skin): The aerodynamic outer shell must resist local pressure distributions, surface buckling, and minor impact loads while maintaining geometric accuracy. It is typically built using balanced ±45° fabrics or biaxial laminates, which provide a good compromise between shear stiffness, in-plane strength, and over curved aerodynamic profiles. To increase the shell's out-of-plane stiffness without excessive mass, thin sandwich panels incorporating lightweight foam or balsa cores are often used, particularly in the mid-span region.

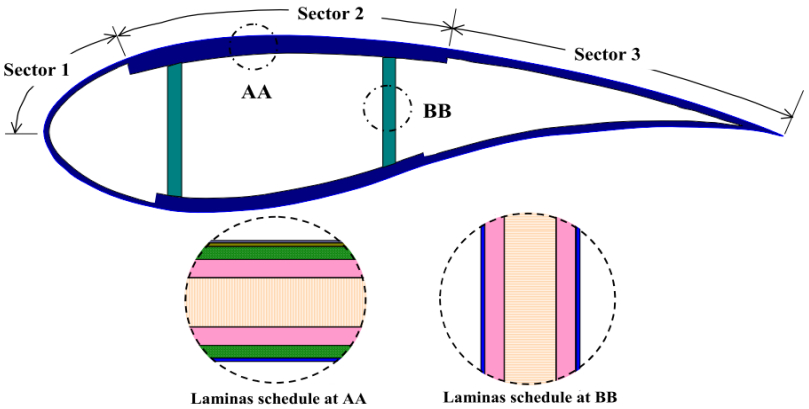

Figure 14: Layup of Blade's section [6]

In summary, the main material used in a wind turbine blade are: Unidirectional carbon fibre laminates; Unidirectional glass fibre laminates; Biaxial and ±45° glass fabrics; Core materials (PVC foam, PET foam, balsa); Gelcoat and surface layers.
The material fraction used is not constant along the blade:

- starting from the Root region, here the bending and shear loads are higher therefore, laminate thickness is greatest here. Unidirectional (UD) fiber layers are thicker, shear webs are strongly reinforced, and core materials are denser in order to prevent shell buckling.
- In Mid-span region the loads decrease, allowing more moderate laminate thickness, sandwich shells become more dominant, and some UD reinforcements decrease.
- Finally Tip region has the lowest loads, so laminates become thinner, cores become lighter, and carbon (if present) is significantly reduced, the goal is to minimise inertia and aerodynamic loads.

This spanwise gradation is fundamental to achieving an optimal trade-off between structural strength, fatigue life, stiffness requirements, and mass minimisation [8].

It's also important to notice that wind turbine blade materials are exposed to environmental factors such as ultraviolet radiation and high humidity, which may result in moisture ingress, absorption, swelling, and changes in material properties. When combined with mechanical loading from rain, wind, and other sources, these environmental effects accelerate the degradation of the blade leading edge.
Erosion together with lightning strikes and manufacturing flaws, is the most critical within the initial five years. Owing to its recurrence, erosion also constitute the most expensive degradation mechanism, primarily because of repeated repair requirements. [9]
Over the past years, multiple approaches to anti erosion coatings have been examined. Among these, thermoplastic and hybrid thermoplastic- based materials have shown considerable potential for the development of highly erosion-resistant coatings. Thermoplastics show more creep and stress relaxation, as compared to thermosets, and that might be one of reasons for the high potential of thermoplastics for leading-edge problem.
In the coating, add particles and other reinforcements can cause the dissipation of stress waves from liquid impact, thus, reducing local stresses, and it can also increase the strength of the coatings. This opens also a path to the development of sustainable, bio-based anti-erosion coatings. Compared to polymers commonly applied in anti-erosion coatings, bio-based polymers generally possess inferior mechanical properties. Nanocellulose fibres, characterised by chemical inertness, high mechanical performance, low density, and dimensional stability, present a highly suitable option for reinforcement in wind turbine blade anti-erosion coatings.

3.5.3 Blade end-life

Apart from the intermittent nature of wind as a resource, one of the major challenges facing the industry is waste management, particularly the disposal of decommissioned blades. As mentioned, these blades are typically manufactured from glass fiber-reinforced polymers bonded with balsa wood using epoxy resins or polymer foams, and in areas subjected to high mechanical stress, carbon fiber reinforcements may also be incorporated. The strong bonding of these hybrid materials is essential for enabling blades to withstand rotational speeds exceeding 250 km/h without damage. However, while this composite design is highly advantageous for energy production, it poses significant challenges at the end of the blade's life cycle, as the separation of the constituent materials is extremely difficult.
One solution is offered by Siemens Gamesa with the new technology RecyclableBlade, that enables the separation of materials at the end of the blade's life cycle, allowing them to be recycled into new applications. These blades are manufactured from a combination of materials bonded with a specially designed resin that provides lightweight, strong and flexible components through a mild process, thereby preserving the integrity of the individual materials.
Another solution is given by Voodin Blade Technology, with its turbine blade made of laminated wood veneer. This product ensures strength, dimensional stability and high load-bearing capacity.

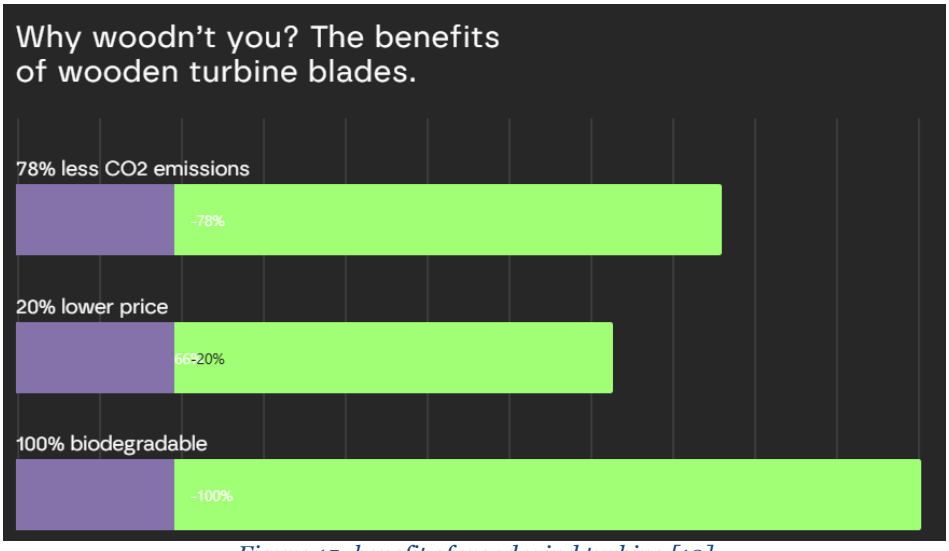

Figure 15: benefit of wood wind turbine [10]

4 Structural optimization framework in Co-Blade

4.1 Introduction to Co-Blade

Co-Blade is an open-source, MATLAB-based framework developed at Sandia National Laboratories for the structural sizing and analysis of large composite blades for both wind and hydrokinetic turbines. By coupling aerodynamic loading, sectional property synthesis (via classical lamination theory), and one-dimensional beam analysis, the tool enables rapid, parametric exploration of design alternatives within a computationally efficient workflow. The primary objective of *Co-Blade* is to accelerate the preliminary design phase by allowing designers to rapidly evaluate alternative laminate layups and assess their impact on blade properties, global deformations, and local stress/strain responses.
In this work, the above objective is operationalized through a data-driven workflow that makes *Co-Blade* immediately actionable. Within this thesis, *Co-Blade* was employed to perform structural analyses and optimization. The required inputs consisted of the blade geometric definition, material properties, and aerodynamic load distributions, together with cost and design constraints. Based on these inputs, *Co-Blade* automatically computed the sectional stiffness and mass matrices using classical lamination theory, with a Euler-Bernoulli theory and shear flow theory applied to composite beams, assembled the one-dimensional beam model, and evaluated the resulting deflections, internal forces, and stresses along the blade. The optimization routine then iteratively adjusted the laminate thicknesses and structural parameters to minimize the objective function (typically the total blade mass or cost) subject to the imposed design constraints. This workflow provided an efficient and reliable foundation for the subsequent aero-structural and techno-economic analyses presented in the following chapters.

4.2 Reference wind turbine

The structural optimization developed within this thesis is based on the IEA Wind 15-MW Offshore Reference Turbine [11].
Reference wind turbines serve as open benchmarks for research and enable consistent comparison between different modelling and optimization methodologies. The IEA 15-MW configuration represents a Class IB, direct-drive, fixed-bottom offshore turbine characterized by a rotor diameter of 240 m, hub height of 150 m, and rated wind speed of 10.6 m s^{-1}.

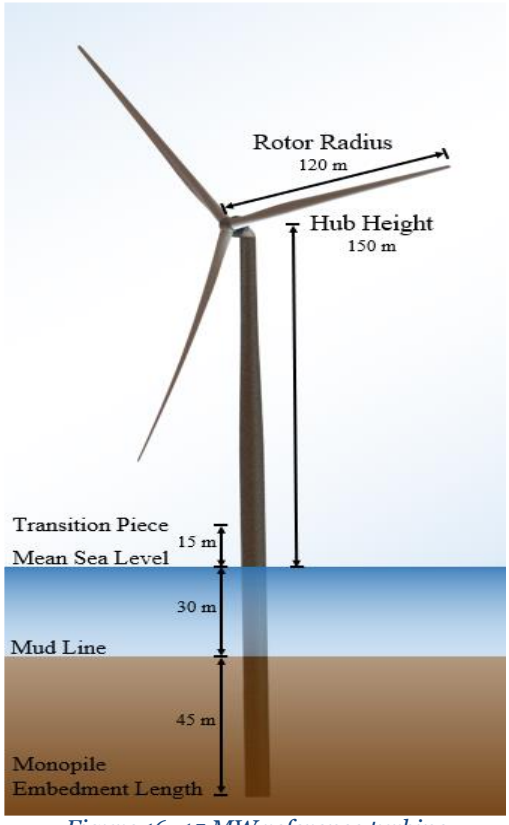

Figure 16: 15 MW reference turbine

The rotor is composed of three 117 m-long blades, each with a root diameter of 5.2 m, maximum chord of 5.77 m at 0.23 R, and a total mass of approximately 65 t.
The turbine operates at a design tip-speed ratio of 9, achieving a power coefficient of 0.489, and employs a DTU FFA-W3 series of airfoils, specifically FFA-W3-211, 241, 270blend, 301, 330blend, 360, and SNL-FFA-W3-500 near the root.

Table 2: Main parameter of reference turbine

Parameter	Symbol	Value	Unit
Rated Power	P_{rated}	15	MW
Rotor diameter	D	240	M
Blade length	L_b	117	M
Hub radius	R_{hub}	4	M
Rated wind speed	v_{rated}	10.6	m/s
Tip-Speed ratio	λ	9	-
Hub height	H_{hub}	150	M
Blade mass	m_b	65	ton

4.2.1 Structural Configuration and Material Definition

The structure of the IEA 15-MW reference blade is based on a conventional large-scale composite architecture, designed to achieve an optimal balance between stiffness, strength and manufacturability. The layout consists of two primary load-carrying spar caps made of unidirectional carbon fiber composites (UD-Carbon), providing high longitudinal stiffness with minimal weight contribution. One located on the pressure side and the other one on the suction side of the airfoil.
The spar caps are connected by two shear webs, which extend from approximately 10% to 95% of the blade span, ensuring torsional stability and efficient load transfer between the pressure and suction sides. The webs are made of unidirectional glass fiber laminates (UD-Glass). Between the spar caps, the webs and the leading/trailing edge reinforcements foam filler panels are inserted on both sides of the blade to form sandwich skins, enhancing the out of plane stiffness and reducing overall weight.

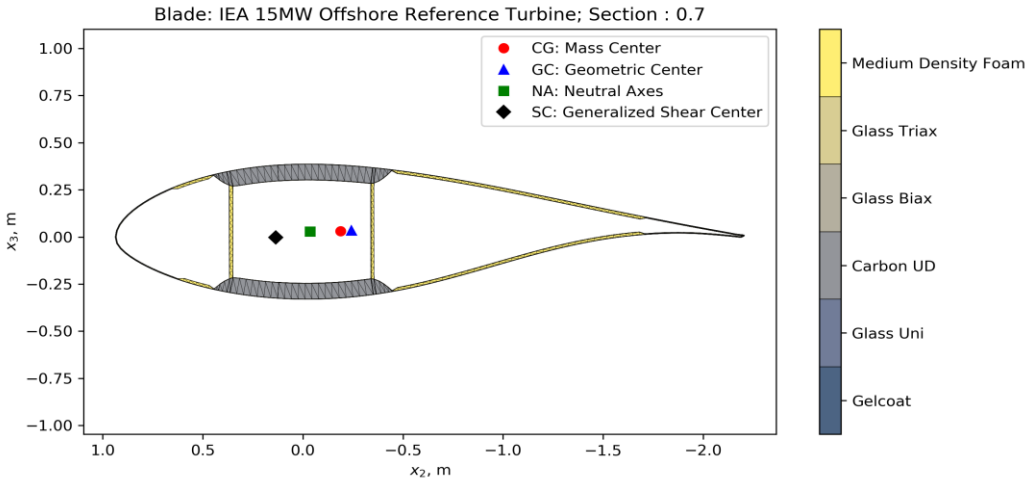

Figure 17: structural configuration of the blade

The materials used in Co-Blade have been reduced to minimise computational work. In the table below are show the used materials, each characterized by its in-plane elastic moduli, Poisson's ratio, density and allowable tensile and compressive stresses.

Table 3: material properties

ID	**Material**	$E_{11}[Pa]$	$E_{22}[Pa]$	$G_{12}[Pa]$	$v_{12}[-]$	$\rho[\frac{kg}{m^3}]$
1	Biaxial Glass	1.34×10^{10}	1.34×10^{10}	1.21×10^{10}	0.53	1910
2	UD-Glass	4.32×10^{10}	1.26×10^{10}	4.42×10^{10}	0.29	1926
3	UD-Carbon	1.29×10^{11}	7.62×10^{9}	3.81×10^{9}	0.32	1548
4	Foam Core	1.30×10^{8}	1.30×10^{8}	5.00×10^{7}	0.32	130

Within Co-Blade, these materials are defined in the input database as separate layers, each associated with its corresponding thickness, orientation, and position along the blade cross-section.
The UD-Carbon layers in the spar caps carry the primary flapwise bending loads, while the UD-Glass in the shear webs contributes to torsional rigidity and shear transfer. The Biaxial Glass skins provide shell stiffness and improve fatigue performance, and the Foam Core ensures geometric stability of the sandwich panels at minimal mass penalty.
This structural configuration and material definition constitute the baseline model implemented in Co-Blade, serving as the starting point for the frozen-loads optimization phase.

4.3 Frozen Loads Optimization setup and results

4.3.1 Optimization setup

The first optimization step is the Frozen Loads Optimization, which consist of a preliminary stage in the overall design process. In this phase, the aerodynamic loading and geometric configuration of the blade (chord, airfoil thickness, twist angle) are keeping constant, evaluated at the rated operating condition (v_{rated} =10.6 m/s), while only the structural variables are allowed to change (thickness of Spar Cap, Outer / Inner shell and Foam).
This approach makes possible to efficiently investigate the influence of the composite layup, material selection, and spar cap geometry on mass, cost and structural margins, without the computational overhead associated whit aero structural coupling.
The Optimization phase start with the Frozen Loads strategy for multiple reasons like, it establishes a controlled environment for model verification, since the aerodynamic input is fixed and well defined, deviations in result are attributed to structural or

material modelling. Another, and more important, reason for starting the optimization whit frozen loads is that delivers a robust baseline configuration, a structurally optimized blade consistent with the rated aerodynamic load distribution, that can subsequently be used as the starting point for the aero-structural optimization stages.
The final objective of this optimization is to reduce the total blade cost (M€), while ensuring compliance with structural constraints on tip deflection, frequency, material stress and local buckling. The optimization problem is:

$$\min_{x} C_{blade}(x)$$

Whit constrains:

$$\begin{cases} \delta_{tip} < \delta_{\max} = 20\ m \\ f_1 \geq f_{\min} = 0.450\ Hz \\ \lambda_{buckling} \leq \lambda_{\max} = 0.5 \\ \sigma_i \leq \sigma_{\max} = 0.25\ MPa \end{cases}$$

Where x denotes the laminate thickness distributions of the spar caps, webs, shell, and foam-core regions, then:

- C_{blade} is the total blade cost,
- δ_{tip} is the tip deflection,
- f_1 the first natural frequency,
- $\lambda_{buckling}$ the local buckling factor.

These constraints are the minimum features for a realistic overview of the blade.
The tip deflection represents the downwind displacement of the blade tip under the applied aerodynamic loading, so excessive deflection can lead to several undesirable effects like, tower violation, where the blade approaches the tower during rotation, or increased fatigue loading, arising from larger oscillatory motions.
The first natural frequency denotes the fundamental flapwise bending mode of the blade, computed from the sectional stiffness and mass properties. Maintaining adequate separation between the blade's structural frequencies and rotor excitation frequencies (1P, 3P…) is essential to avoid resonance, which would drastically increase cyclic stresses and compromise fatigue life. This constraint guarantees that the optimized blade remains dynamically stable during operation.
The buckling factor ensures that local shell and panel instabilities remain safely below critical conditions, this is particularly important considered that thin composite panel experience high compressive stresses near mid-span.
Last, the stress constraint referred to all the type of stress in each composite layer (tension, compression, shear and transverse stress). These are evaluated along the span and through the thickness using the lamination theory implemented in Co-Blade. By enforcing a maximum stress, the optimization ensures that the structural

configuration remains safe under rated loading conditions.
Together, these constraints ensure that the optimized configuration not only achieves a reduction in manufacturing cost, but also maintains structural integrity, stability, and dynamic compatibility with the turbine's operating environment.

All this optimization routine was implemented in MATLAB via the particle swarm function, which employs a population-based stochastic algorithm inspired by swarm intelligence. Meaning, it uses a population of particles that search is best personal position and the best swarm position. This iterative process allows the swarm to converge on optimal or near-optimal solutions. This approach proved robust in avoiding premature convergence and ensuring global exploration, ultimately providing a stable and cost-effective structural solutions.

4.3.2 Optimization Results

The Frozen-Loads optimization converged to a structurally feasible and cost-effective configuration, whit the total blade cost stabilizing around 0.68 M€, reduced from the initial value of nearly 1.2 M€, after nearly 900 iterations (Figure 18).

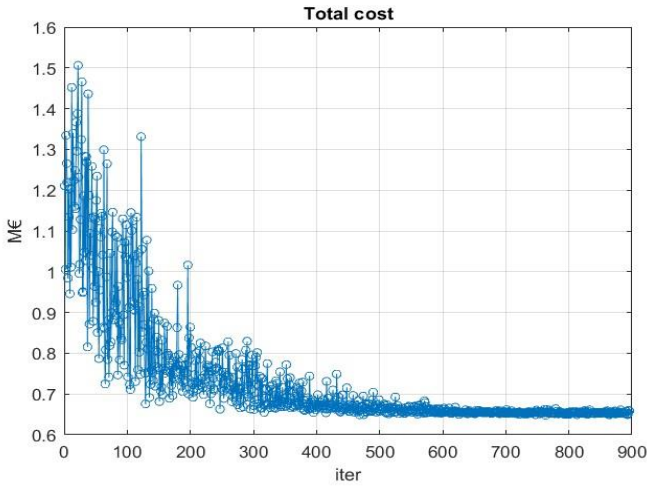

Figure 18: Total blade cost, Frozen-Loads

The initial phase of the particle swarm function is more an exploration phase, in the first 150 iterations, then follow a slower refinement stage as structural constraints became active and guided the design toward feasible regions.
One constraint-driven behaviour is the evolution of the tip deflection, reported in Figure 19.
In the initial iterations, the deflection is relatively low, between 10 and 14 m, reflecting the higher stiffness of the starting configuration.
With the aim of reducing total costs, optimisation reduces laminate thickness, resulting in an increase in tip displacement to approximately nineteen metres, near

to the maximum allowable downwind deflection imposed by constraint.

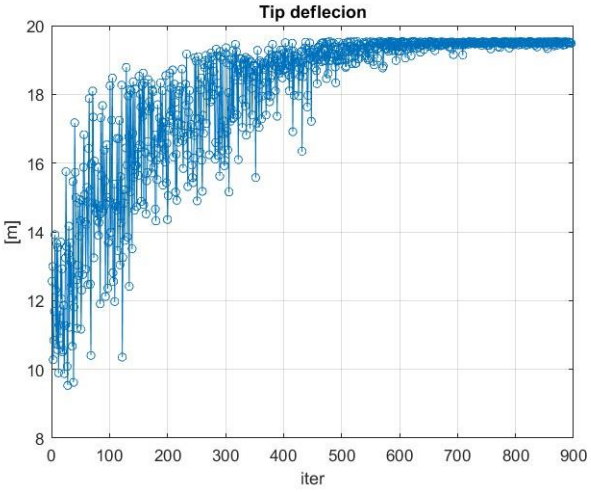

Figure 19: Tip deflection, Frozen-Loads

This behaviour is directly linked to the spanwise distribution of spar cap stiffness, which represent, first the primary contributor to flapwise bending rigidity in large composite blades, and second of all, being made of unidirectional carbon fiber, is the most expensive material used in the blade structure.
In the present implementation, the spar cap thickness, as well as outer/inner shell, foam and web thickness, is not defined continuously along all spanwise stations, but rather through six key point located at predefined positions. During each iteration, Co-Blade linear interpolates the thickness between these control points to generate a continuous profile along the full 117 m blade span.
During optimization, the particle swarm systematically adjusts their thickness to satisfy the deflection constraint, in fact the inboard regions (0-25 m) retain relatively thick spar cap laminates, as these section contribute most of the global bending stiffness, whereas outboard regions experience more aggressive thickness reductions, where the structural leverage is smaller and material removal has a stronger impact on cost than on stiffness (Figure 20).

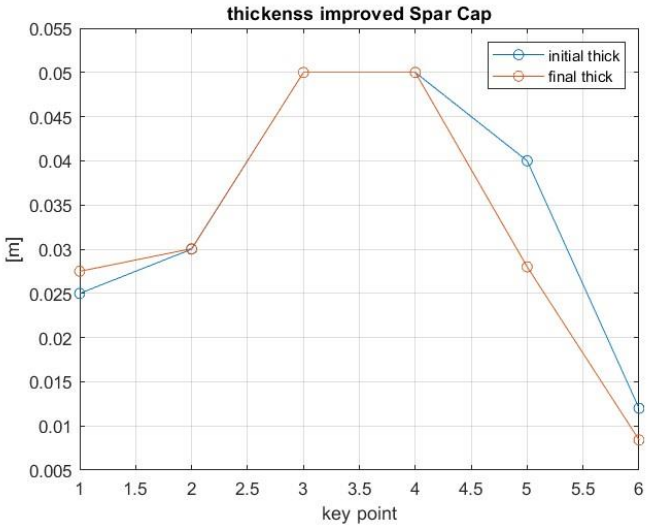

Figure 20: Improved thickness of Spar Cap, Frozen-Load

This redistribution explains the monotonic increase in tip deflection across the iterations: the optimization algorithm progressively reduces spar-cap thickness toward the mid- and outboard regions until the structural stiffness approaches the minimum required to maintain compliance whit the allowable tip displacement.
The final configuration thus reflects a structurally efficient layout in which inboard spar caps are sized by stiffness, and outboard spar caps are sized by cost.
In addition to tip deflection, two other global indicators provide valuable insights into the evolution of the structural configuration along the optimization process: the flapwise natural frequency and the total blade mass.
Both quantities evolve consistently whit the progressive reduction in structural stiffness associated with cost minimization.
The evolution of the natural frequency is reported in Figure 21. As for the tip deflection, at the beginning of the optimization, the frequency and the total mass, exhibits significant variability, due to the wide exploration of the design space performed by the particle swarm.
As the algorithm converges, the frequency stabilizes around 0.49-0.50 Hz, remaining above the minimum allowable value required to ensure sufficient separation from the rotor excitation frequencies (1P and 3P).

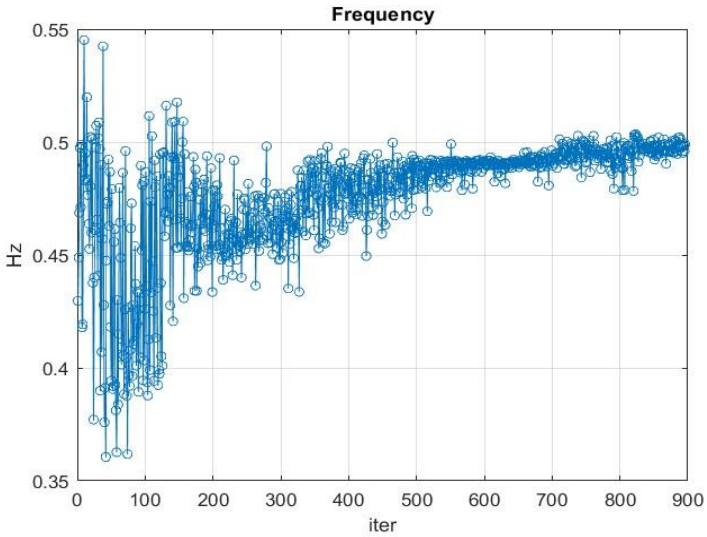

Figure 21: Frequency, Frozen loads

The total mass of the blade, shown in Figure 22, follows a trend like the cost evolution. The initial configuration exhibits a mass higher than 110 tons, which progressively decreases as unnecessary material is removed from the outboard and mid span regions, reaching a value of approximately 65-66 tons. This value is consistent with the mass range typically reported for 15 MW class blades and confirms that the optimizer successfully identifies a structurally feasible configuration with significantly reduced material usage compared to the initial case.

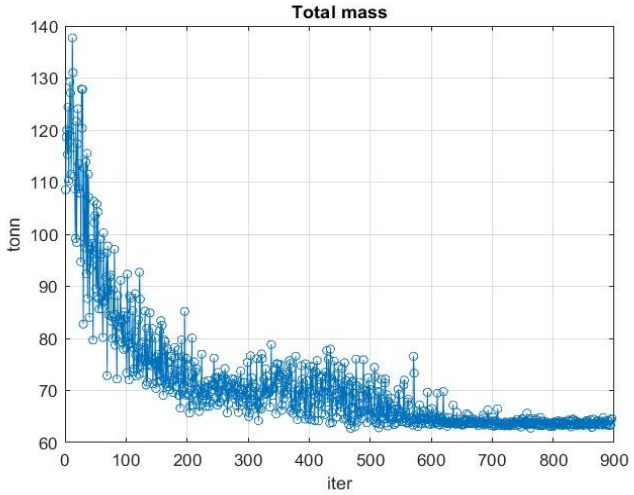

Figure 22: Total blade mass, Frozen Loads

The combined evolution of frequency and mass illustrates the trade-off managed by the optimizer: as material is removed to reduce cost and mass, the structural stiffness is adjusted until further reductions would either violate the allowable tip deflection

or bring the natural frequency too close to the excitation range. The optimization converges when further material reductions would violate some constraints, thereby identifying the minimum cost configuration that still meets all structural requirements.
Another interesting interaction between structural behavior and constraint reinforcement is highlighted by the buckling safety factor in Figure 23. Co-Blade discretizes the blade into 30 sections, each representing distinct structural slice along the 117 m span. For each of these sections, the software computes the local stiffness matrices, stress fields, and the corresponding local buckling factor, resulting in the spanwise curve show in the Figure 23. Each point of the plotted curve therefore corresponds to one of the 30 structural stations of the beam model. The two peaks represent the points under the most stress and therefore more sensible to "instability", while remaining within the limit of 0.5, ensuring that local instability remains safely below the critical threshold across all stations.

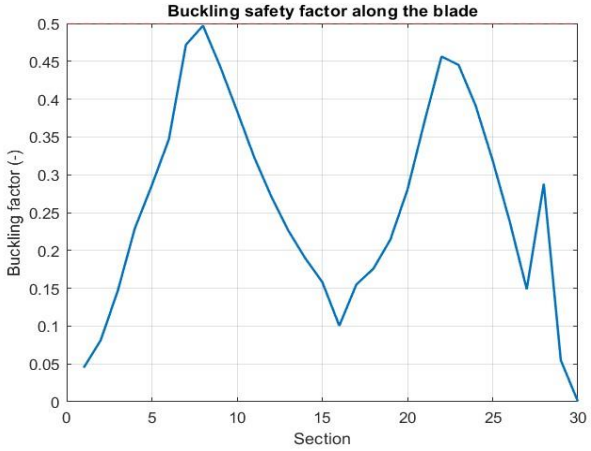

Figure 23: Buckling along the blade, Frozen Loads

The influence of the material strength constraints can be assessed through the normal strain field, shown in Figure 24. The map of the blade exhibits the expected asymmetry between pressure and suction sides: tensile strains develop mainly in the pressure side spar cap, whereas compressive strains appear in the suction side spar cap. The smooth variation of ε_{11} along the span and around the circunfaerence suggests that no discontinuities or localised hotspots are introduced by the optimizes layup.

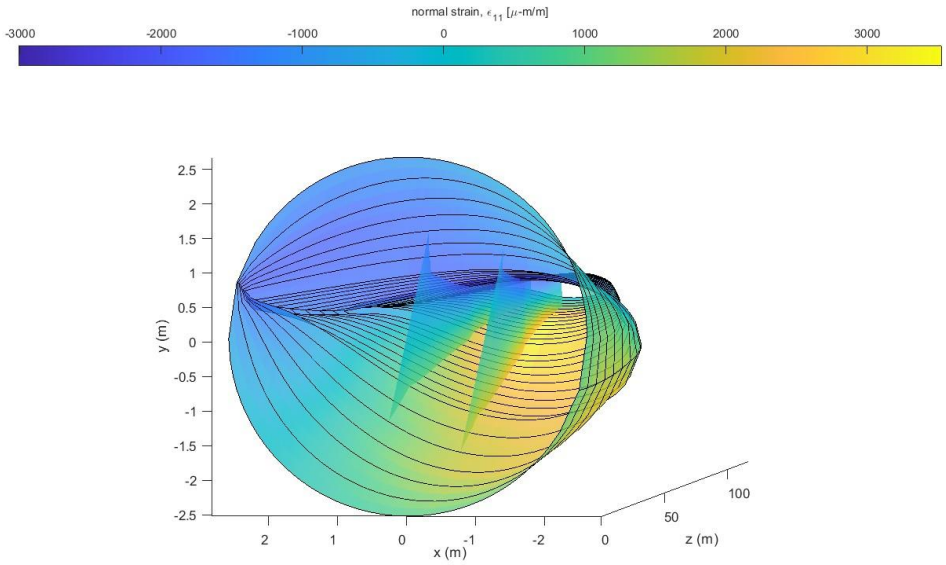

Figure 24: Normal strain ε_{11}, Frozen Loads

Overall, the combined interpretation of cost convergence, deflection behavior, natural frequency, mass evolution, buckling response and normal strain distribution demonstrates that the frozen loads optimization successfully identifies a structurally sound and economically efficient baseline configuration. This optimized configuration serves as robust starting point for the subsequent aero-structural optimization, where geometric and aerodynamic parameters will be incorporated as additional degrees of freedom.

4.4 Aero-Structural Optimization

Following the frozen loads optimization, the next step is the aero-structural optimization framework. In contrast to the previous stage, where geometry was fixed and only the structural layup was optimized, this second phase allows simultaneous modification to both the aerodynamic geometry and the structural configuration of the blade.
Starting whit, the base of the previous optimization, introducing the Aerodynamic performance (AEP) is necessary, and this is linked to geometry, particularly chord, twist and airfoil thickness distributions. These structural features strongly influence the blade performance and the cost, because they determine loads distribution, stiffness, mass, and buckling susceptibility.
By allowing the blade geometry to vary in parallel with the composite layup, the optimizer can explore a richer design space and identify configurations that simultaneously increase aerodynamic efficiency and AEP, reduce structural mass and material cost, and satisfy all strength, stiffness, buckling and frequency requirements.
To avoid unrealistic or aerodynamically degraded shapes, some penalties are added to the previous one employed in the frozen load optimization, for chord and airfoil thickness:

- $2\,m \leq chord \leq 8\,m$, that ensure manufacturability and compatible aerodynamic loading,
- E $Airfoil\ thickness \geq 0.210\,m$, preventing excessively thin sections that would collapse structurally.

A penalty for the twist angle was also added, although no explicit numerical bounds were necessary, but a penalty for ensuring a monotonic decrease towards the tip. This monotonicity is important for avoid unphysical operating conditions, and load distributions incompatible with smooth BEM convergence.

4.4.1 Aerodynamic Model and Load Evaluation

Now the full optimization problem includes a set of geometry and structural variables, which defines a multidimensional design space large enough to capture the characteristics of coupled blade behaviour while still allowing feasible convergence in a PSO-based algorithm.
At each iteration of the optimization, the aerodynamic loads are recomputed to reflect the updated blade geometry.
This dynamic coupling ensures that every geometric modification is immediately translated into aerodynamic performance variations.
The updated geometry alters the local Reynolds numbers, lift and drag coefficients and inflow angles, adjusting the magnitude and distribution of aerodynamic loads.
Once the distributed aerodynamic forces are obtained, the complete power curve of the rotor is rebuilt.

The Annual Energy Production is then computed by integrating the power output over the representative wind-speed distribution.
Through this procedure, AEP becomes an explicit component of the optimization loop rather than a post-processing metric, thus ensuring that any geometric or structural modification is evaluated in terms of its energy performance.
In the Frozen Loads optimization, the objective function was the total blade cost, now in this aero-structural framework, the objective became the Cost-to-AEP ratio, an indicator that directly reflects the economic efficiency of the blade:

$$\min\left(\frac{Total\ Blade\ Cost}{AEP}\right)$$

The choice of this metric shifts the design philosophy toward a techno-economic perspective aligned with the Levelized Cost of Energy.

4.4.2 Aero-structural Results

The introduction of geometry as an active component of the optimization process changes the behaviour of the blade, both aerodynamically and structurally, and the results obtained from the coupled simulation framework highlight this mutual dependence.
During this stage, every iteration of the particle-swarm algorithm triggered a full re-evaluation of the aerodynamic performance and of the structural response. The converged configuration thus represents the equilibrium point at which aerodynamic efficiency and structural feasibility coexist under the minimization of the Cost/AEP objective function, that numerically correspond to nearly 11.6 €/MWh. A significant reduction from the initial value for the 15 MW reference turbine (without optimization) of approximately 13.5 €/MWh.
The overall trend of this convergence is visible in the evolution of total cost and AEP, which are reported in Figure 26 and in Figure 25 respectively.

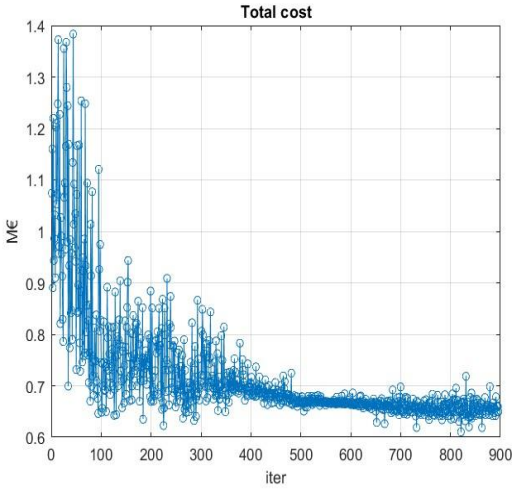

Figure 26: Total blade cost, aero-struct opt

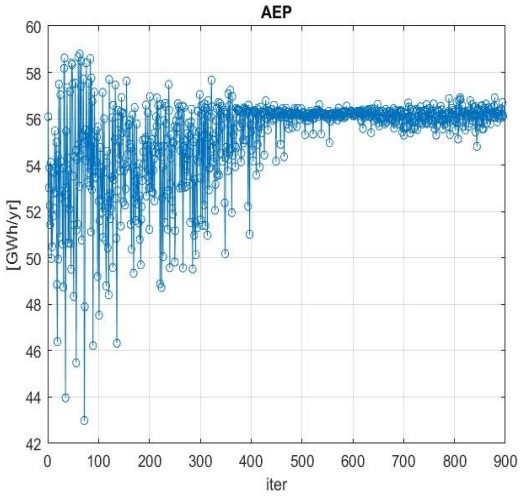

Figure 25: AEP, aero-struct opt.

From the aerodynamic point of view, the geometric distribution of chords, twist and airfoil thickness define the performance of the blade across the wind-speed spectrum. The optimized chord profile, shows in Figure 27, displays a more aerodynamically favorable distribution: compared to the baseline (red line), the inboard region is reduced, reflecting a decrease of approximately 10-15 %, whereas the outer half of the blade exhibits a modest increase, particularly beyond mid-span. The redistribution tends to reduce excessive aerodynamic loading near the root, while enhancing lift generation where the blade experiences more favorable inflow conditions.

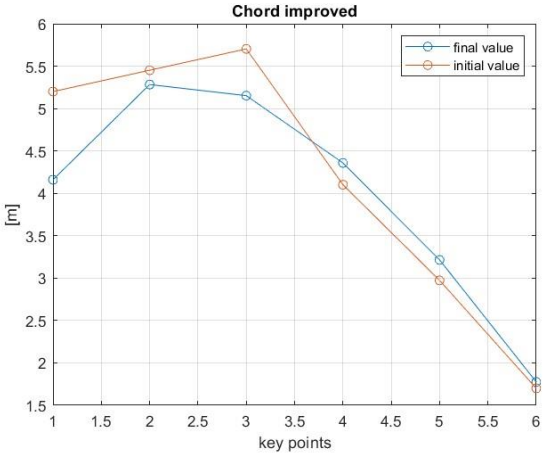

Figure 27: Chord, aero-struct opt.

The twist distribution evolves quite the same. As shown in Figure 28, the optimized twist shows a modest increase inboard, followed by a more gradual decrease toward the tip. These adjustments improve the spanwise angle-of-attack distribution, moderating high-load regions while enhancing performance in mid-wind regimes.

The monotonicity penalty ensured the absence of twist reversals, giving rise to a smooth and physically consistent profile.

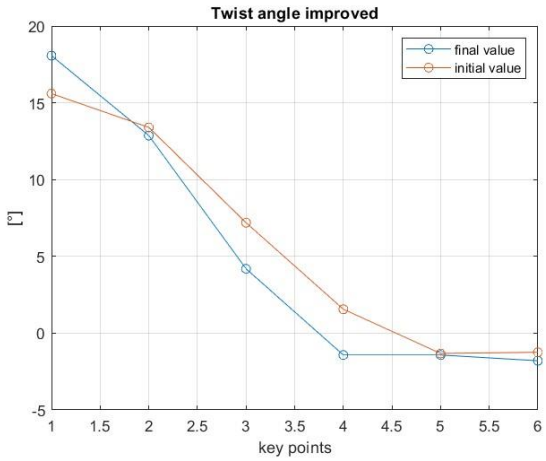

Figure 28: Twist angle, aero-struct opt.

Complement to these modifications, the airfoil thickness distribution undergoes a progressive thinning, observable in Figure 29.
Toward the tip, the optimized configuration approaches the minimum allowable thickness of 0.210 m, nevertheless is lighter than the initial case because of the thin reduction in the inboard section. By decreasing the airfoil thickness inboard, the optimization successfully reduces weight without compromising overall structural performance or aerodynamic efficiency, while thicker airfoils toward the tip contribute to the blade's ability to handle larger aerodynamic forces and increase its performance in high-wind conditions.

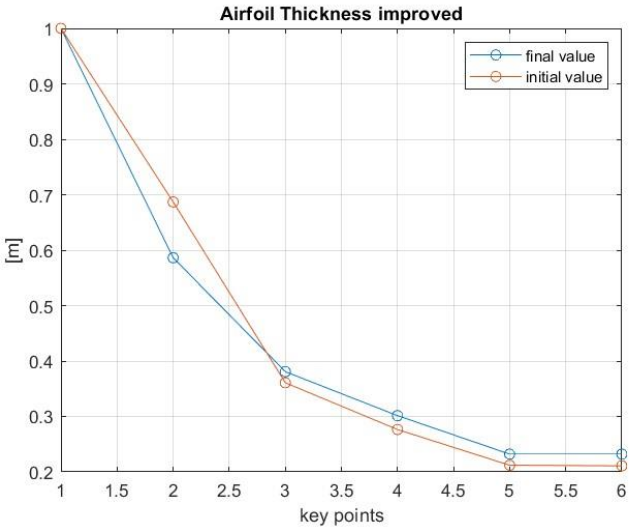

Figure 29: Airfoil thickness, aero-struct opt.

These geometric modifications immediately influence the structural configuration, beginning with the redistribution of spar-cap thickness. The optimized spar-cap profile, shown in Figure 30, exhibits a concentration of stiffness in the inboard region, where bending loads dominate.
Further outward, the spar-cap thickness decreases, up to 30-40% in some areas, allowing the blade to achieve significant material saving (Carbon UD, the more expensive one) without compromising overall stiffness requirements.

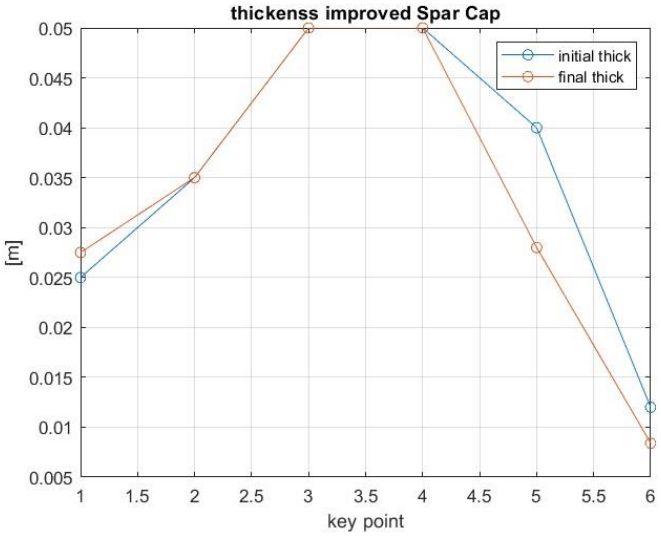

Figure 30: Spar-Cap thick, aero-struct opt.

These structural modifications are mirrored in the global mechanical response of the blade.
The deformation shape of the blade is shown in Figure 31, where the undeformed blade is represented in black and the deformed one is represented in red. The deformation increases progressively from the root toward the tip, at demonstration that no localized distortion or abrupt changes in curvature are present. This shows that the deformation is wide inside the 20 m constraint.

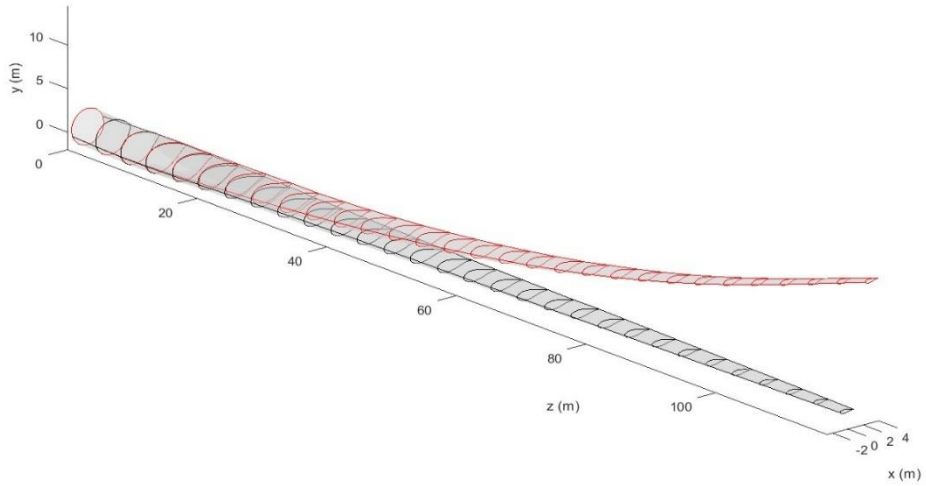

Figure 31: Blade deflection, aero-struct opt.

The normal strain distribution resulting from the aero-structural optimization is shown in Figure 32, showing a smoother and homogeneous pattern along both the suction and pressure sides. Like for the frozen load result, the strain distribution is defined by compressive strains on the pressure side and tensile strains on the suction side. But, whit respect to the frozen-load case (Figure 24), the overall value of the strain is much lower, because before the geometry was fixed and only the laminate thickness could vary, which resulted in higher local strain peaks and in more pronounced strain gradients near the inboard region and close to the shear-web attachments.
Once the geometry becomes part of the design space, the optimizer can act simultaneously on chord, twist, airfoil thickness and laminate thickness. These additional degrees of freedom enable the blade to redistribute both stiffness and aerodynamic loading, leading to a strain field that is more uniform and less picked.

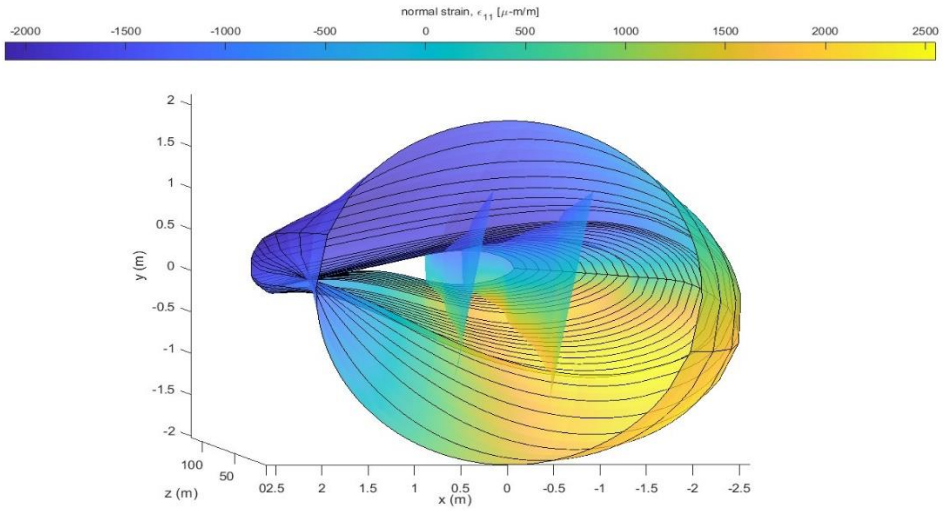

Figure 32: Normal strain, aero-struct opt.

Finally, the buckling distribution, shown in Figure 33, remains two local maximum but satisfies the imposed limit of 0.5 at every section of the blade.

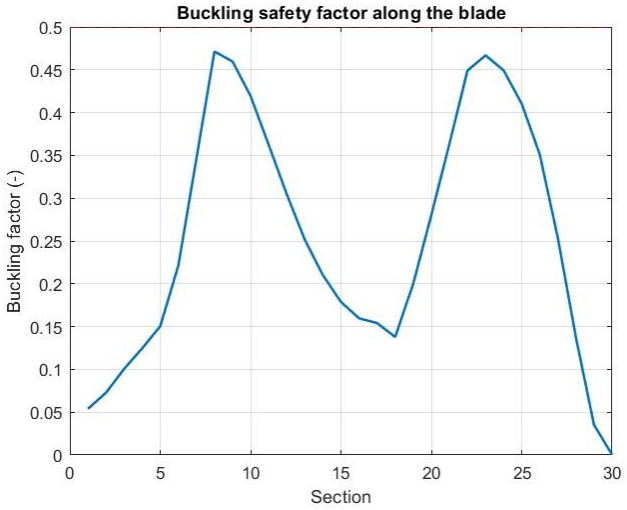

Figure 33: Buckling, aero-struct opt.

Taken together, these results demonstrate that aero-structural optimization has produced a blade that is simultaneously lighter, and more aerodynamically efficient and structurally balanced.
This optimized configuration establishes the foundation for the subsequent analysis that born from the question: “these results are randoms? Or the optimization is strong and so there isn’t big change from one particle warm iteration to another?”

4.5 Analysis of the optimization Robustness

The optimization procedure adopted in this thesis relies on a Particle Swarm Optimization (PSO) algorithm, a stochastic population-based method whose solution depends not only on the starting data, but also on the randomized process.
For this reason, despite the convergence of results, there is no certainty that the solution obtained is unique. To analyze whether the results obtained in the aero-structural optimization are correct, and not simply the result of a random optimization that "went well", five independent runs were performed at the same wind speed, each starting from a different initialization of the PSO particles.
Basically, five PSO runs were performed, with approximately 900 iterations for each run, meaning that a total of approximately 4,500 blades were created.
The aim of this analysis is therefore:

- To evaluate how consistently the PSO converges to similar techno-economic performance metrics (Cost and LCOE),
- To examine the variability of structural constraints across the different runs.

4.5.1 Variability of the Cost and LCOE across runs

The first indicator of robustness is provided by the best blade cost computed for each run reported in Figure 34.
Despite the inherent randomness of PSO, the cost values cluster within a relatively narrow band, ranging from approximately 0.545 M€ to 0.645 M€.
This spread, though not negligible, remains acceptable for a stochastic optimization process involving highly coupled aero-structural variables. The decrease observed in runs 3 and 4 highlights the ability of the optimizer to occasionally reach more favorable combinations of geometry and material layout, indicating the presence of alternative local optima with better cost performance.

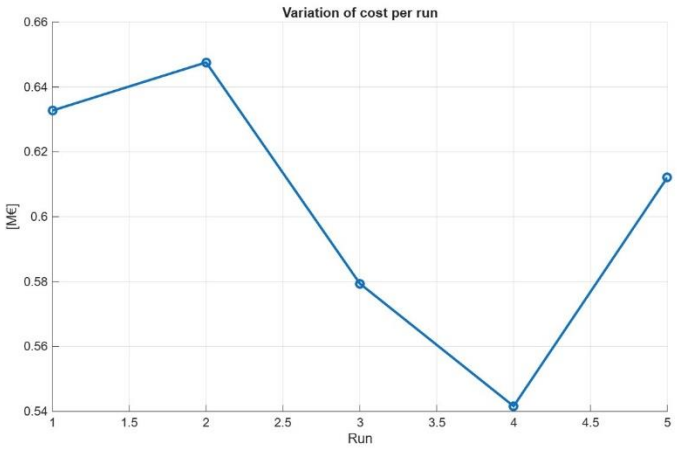

Figure 34: Cost variation per run

A more complete evaluation is given by the Levelized Cost of Energy (LCOE), objective function of the PSO, which directly relates the blade's cost to its aerodynamic productivity.
The techno-economic behavior of the five optimized solutions is first examined through the non-penalized LCOE, reported in Figure 35. The variation across the five runs remains moderate, with values spanning approximately 9.8-13.3 €/MWh, indicating that PSO consistently converges toward economically favorable regions of the design space, even though each run follows a different stochastic trajectory. Further confirmation of stability is provided by the average value of this analysis (mean LCOE ≅ 11.6), which corresponds to the minimum value obtained in the previous optimization analysis.

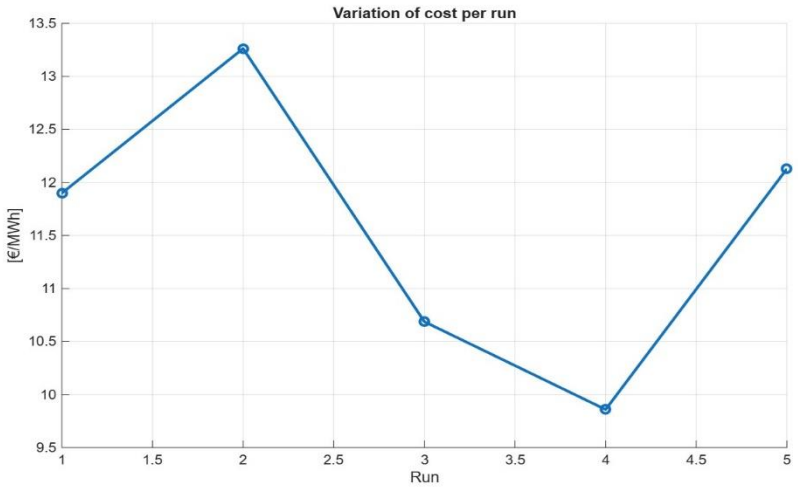

Figure 35: LCOE variation per run

A complementary and more informative perspective is provided by the scatter distribution in Figure 36, where each point represents each blade generated during the optimization process. The vertical axis reports penalized LCOE, i.e. the effective techno-economic performance after accounting for constraint enforcement. The color scale, instead, represents the non-penalized LCOE. This combined visualization clearly shows how constraint enforcement governs the structure of feasible design space. Although many geometries exhibit a low non-penalized LCOE, only a small fraction of these solutions remain admissible once structural and aerodynamic constraint are applied. The optimization process therefore converges toward a compromise region, where cost and energy performance are balanced against the necessity of meeting all structural constraints, (35-40 €/MWh, as shown in Figure 37).

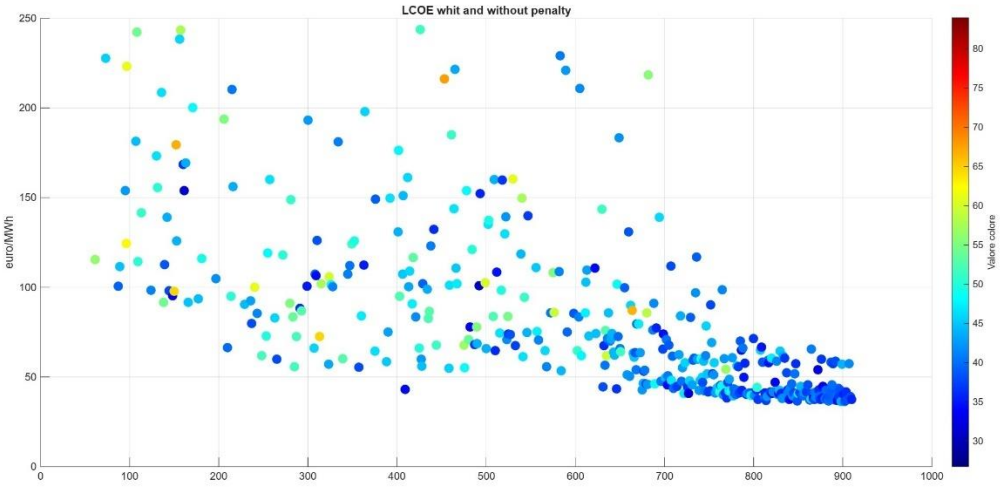

Figure 36: LCOE color map

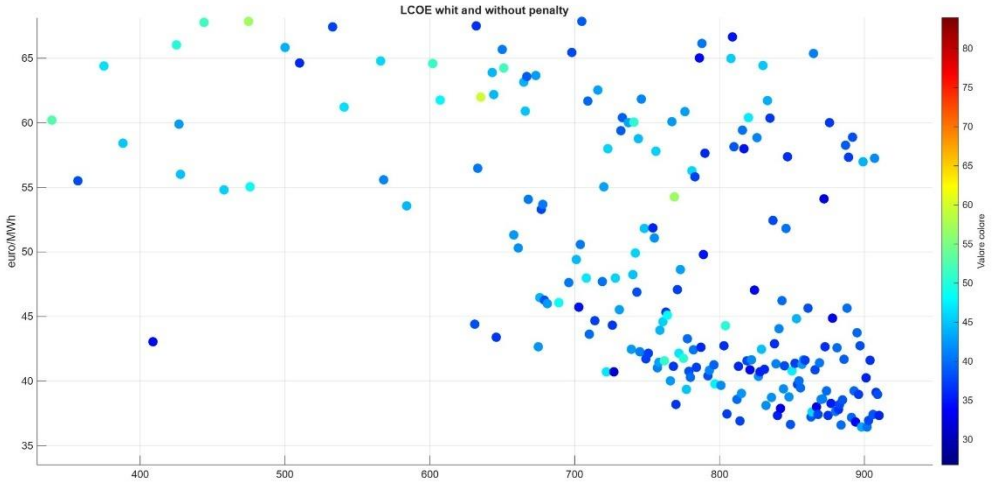

Figure 37: LCOE color map zoom

4.5.2 Structural behavior

Alongside economic consistency, robustness requires that all runs satisfy the aero-structural constraints with similar structural performance. The analysis considers the initial three constraints: natural frequency, tip deflection and maximum stress.
The natural frequency shows extremely limited variability among runs, ranging from approximately 0.443 Hz to 0.455 Hz. All solutions remain very close to the target threshold of 0.45 Hz, with only Run 5 surpassing it. This narrow band indicates that the optimizer systematically identifies geometries with comparable global stiffness.

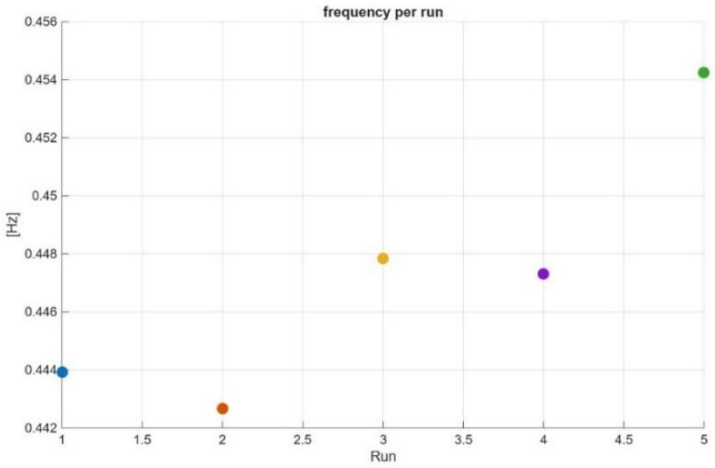

Figure 38: Frequency per run

Tip deflection also shows a similarly compact range, between 12.2 m and 12.9 m. Even though the aerodynamic variables change between runs, the resulting bending stiffness remains consistent across all solutions. This suggests that the penalty system effectively directs the convergence toward structurally feasible blades.

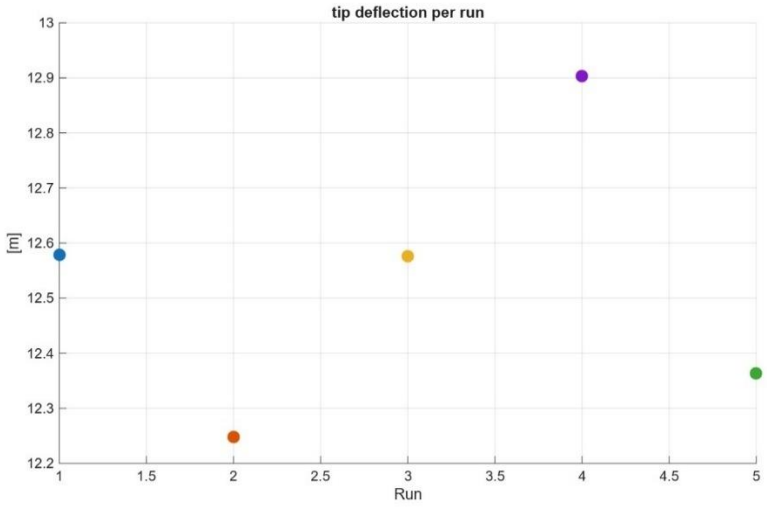

Figure 39: tip deflection variation per run

Last, the maximum stress along the span, for the best blade for every run, is concentrated between 0.23 and 0.25 MPa. These small variations confirm that the optimizer does not exploit unsafe regions of the design space, remaining in a narrow range under the maximum limit of 0.25 MPa.

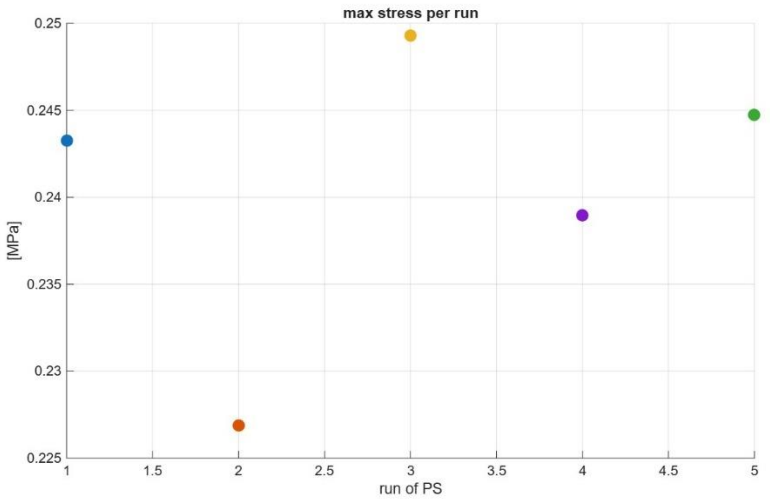

Figure 40: Stress max per run

Overall, the structural consistency across runs demonstrates that the constraints inserted in in the objective function successfully regulate the underlying mechanics of the blade, preventing divergent or structurally anomalous solutions.

4.5.3 Geometric behavior

To understand the source of the small economic variations observed, the geometric output of the five runs is examined. The three main geometric parameters are compared, between runs, across the key points defining the blade.
Starting with the twist angle profiles that remain coherent across runs, especially in the mid-span region where aerodynamics and structural bending interact most strongly. To notice all the profiles, maintain a monotonic decrease toward the tip, obtaining so feasible blade for each run.

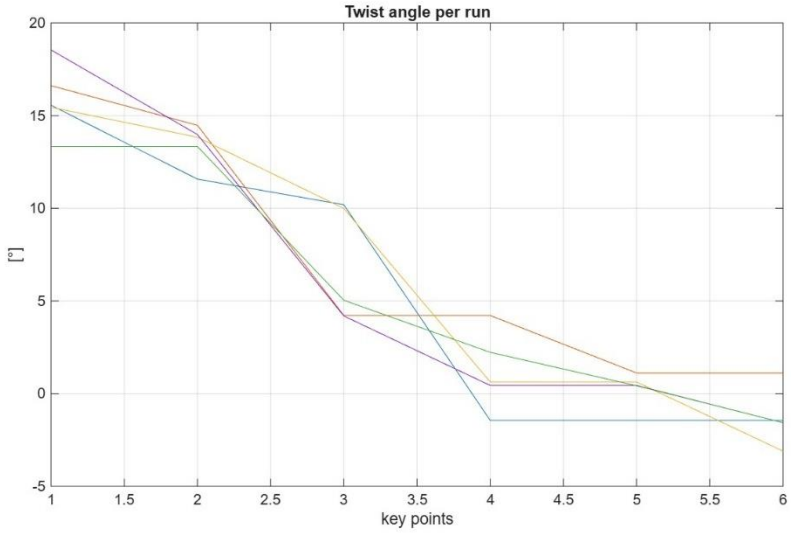

Figure 41: Twist angle comparison

The airfoil thickness distributions exhibit small differences, particularly inboard where structural requirements are dominant. All runs converge toward similar thick root sections and comparable mid-span value, with only minor variations near the tip.

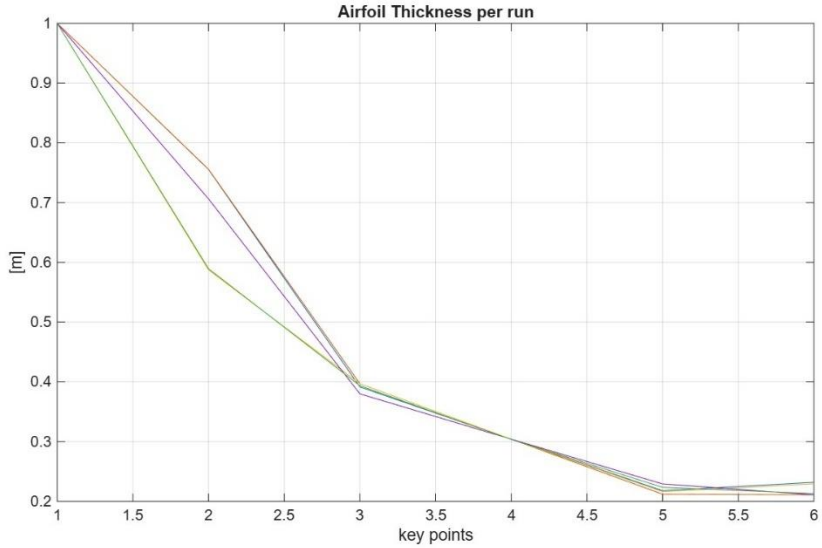

Figure 42: Airfoil thickness comparison

The chord distribution shows the largest relative variability among geometric variables yet remains bound between the enforced limits. The five solutions exhibit similar general trends, moderate inboard chords, a peak near 30-35 % span, and a progressive reduction toward the tip, but with small shifts in magnitude that explain the differences in cost observed among run in Figure 34.

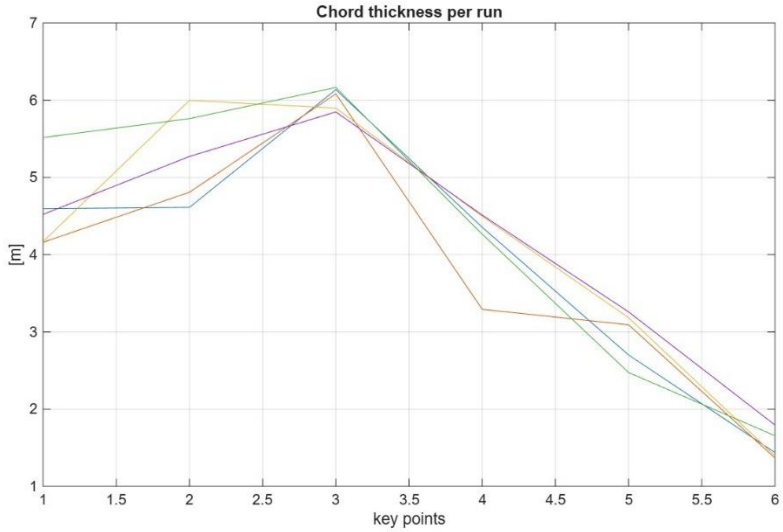

Figure 43: Chord comparison

Examining these three geometric features confirms that the optimizer explores a portion of the design space where different geometric combinations produce similar

structural behavior but slightly different aerodynamic performance. This explains the moderate dispersion in the economic indicators while simultaneously showing that no run diverges towards infeasible geometries.

4.5.4 Conclusion of the optimization robustness

The analysis of robustness demonstrates that the optimization framework behaves consistently across repeated executions. While some geometric variability is observed (mostly in the chord distribution) the structural behavior is nearly invariant, and the economic outputs remain clustered within a relatively narrow range. This combination indicates a stable multi-objective optimization in which several optima coexist, all providing similar trade-offs between cost and energy production.

4.6 Comparison of Optimal Blade Designs Across Different Wind Speeds

After analyzing the robustness of the optimization process, it became possible to extend the investigation by determining the optimal blade configuration for a range of operating wind speeds. Basically, this required running a full Particle Swarm optimization independently for each selected wind regime. Through this approach, it was possible to identify the wind speed at which the blade achieves its most favorable techno-economic performance.
Co-Blade was therefore used to re-optimize the same reference blade at rated wind speeds of 10, 11, 12, 13, 14, 15 and 16 m/s, while maintaining a consistent optimization framework across all cases (objective function, structural and geometric constraints). This systematic procedure allows the quantification of how aerodynamic loading, structural demand and blade cost evolve as the design is progressively modified for increasingly energetic wind regimes. The resulting trends are essential for selecting the most suitable blade design for Mediterranean conditions (typically characterized by moderate and less turbulent winds) as well as for identifying the most appropriate rated speed for blades intended to operate in the more severe environment conditions like the North Sea environment.

4.6.1 Structural response across different rated wind speeds

The first metric investigated is the maximum structural stress reached by the optimized blade at each rated wind speed.

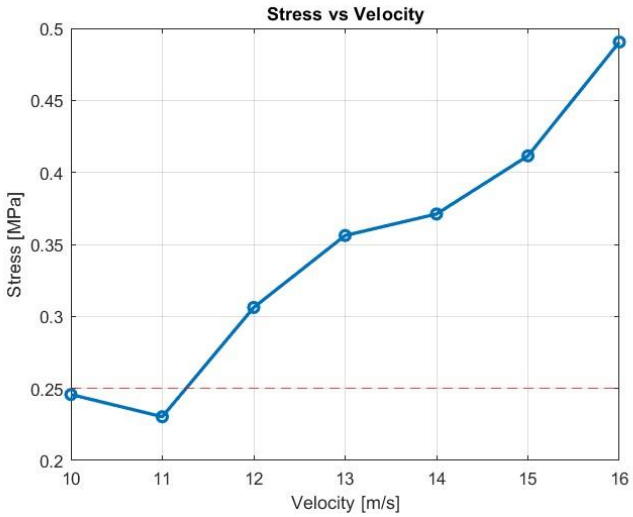

Figure 44: Maximum stress vs velocity

The results show a monotonic increase in stress with wind speed. At 10-11 m/s, the maximum stress lies around 0.23-0.25 MPa, below the allowable limit. However, as rated speed increases, the aerodynamic loads grow significantly, and the stress peaks rise accordingly, reaching almost 0.50 MPa at 16 m/s. Meaning that the optimizer prefers to put some added stress on the blade for a much lower cost-to-AEP ratio. This trend indicates that higher wind-speed designs require considerably stiffer and thicker laminates to maintain structural robustness, and their feasibility becomes increasingly sensitive to fatigue and extreme-load considerations.
The second parameter considered is the flapwise natural frequency of each optimize blade.

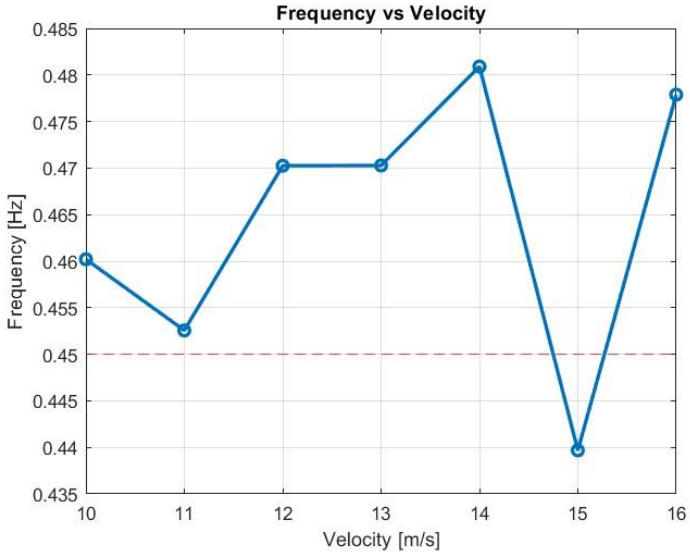

Figure 45: Frequency vs velocity

Across most wind speeds, natural frequency remains above the required 0.45 Hz threshold, indicating that all configurations maintain adequate dynamic stiffness. Only the design optimized at 15 m/s shows a slight dip towards 0.44 Hz, marginally below the threshold. Nevertheless, this deviation is small and can be considered acceptable within typical modelling uncertainties.
Overall, natural frequency remains relatively stable within the range 10-14 m/s, while rated speeds above this range introduce dynamic risks unless additional structural reinforcement is introduced.

4.6.2 Techno-Economic response to different wind speeds

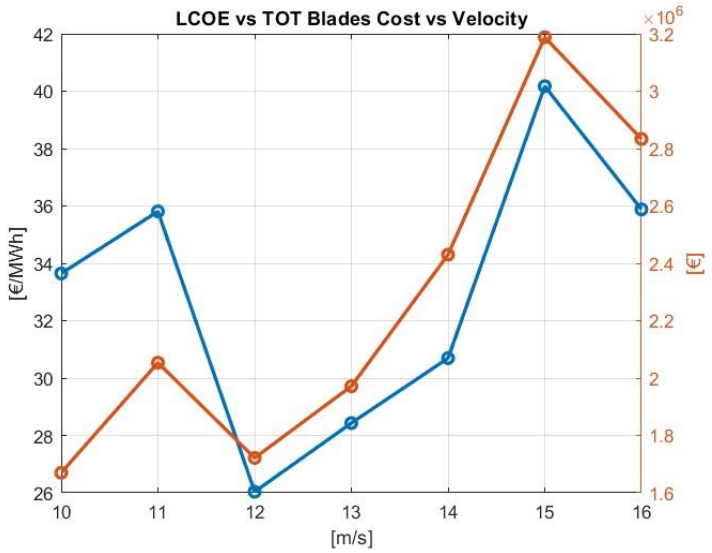

Figure 46: LCOE vs Tot blades cost vs velocity

The total manufacturing cost of the optimized blade shows an increasing trend with higher rated wind speeds. For this graph all three blades of the wind turbine are considered in the analysis of the cost and subsequentially of the LCOE, so the value obtains, basically, represent the cost of the rotor of the turbine. At 10-11 m/s the overall rotor cost is approximately 1.7-2.0 M€. At 12 m/s the cost stabilizes near its minimum, representing the most economical solution among all configurations.
As the rated wind speed rises to 14-15 m/s, the blades cost increases significantly, reaching values around 3.0-3.2 M€, as a direct consequence of the additional material required to maintain structural integrity at higher load levels.
This relationship illustrates a fundamental trade-off: while higher rated wind speeds can potentially increase energy capture, doing so requires a substantially more robust (and thus more expensive) structural design.

More detailed is Figure 47, showing the LCOE for the single best blade for all the velocity, providing the clearest indication of which rated wind speed delivers the best performance.

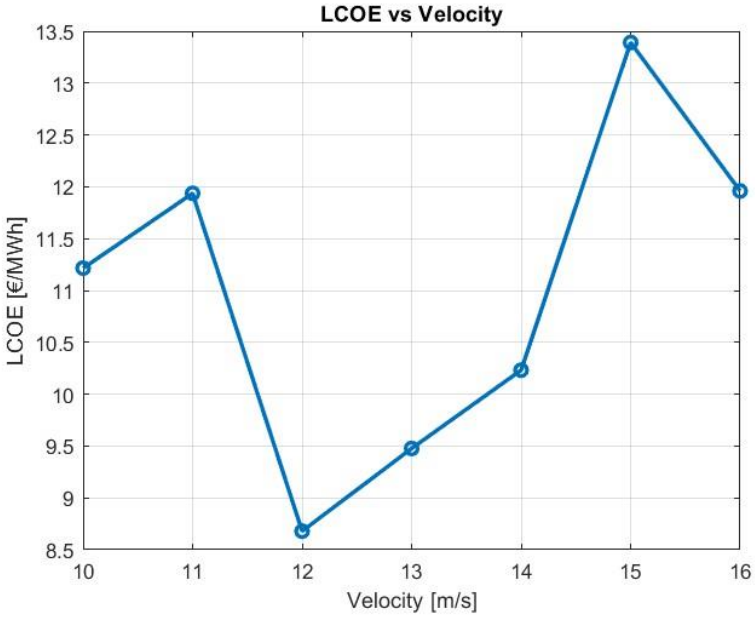

Figure 47: Single blade LCOE vs velocity

The trend obtained from the optimization shows a LCOE minimum at 12 m/s, where the value drops to roughly 8.7 €/MWh, representing the most advantageous balance between structural cost and aerodynamic performance.
At lower rated speeds (10-11 m/s) the LCOE is slightly higher (11-12 €/MWh), primarily due to the reduced energy gathered despite the lower structural cost.
At higher rated speeds (14-16 m/s) the LCOE increases up to 13.5 €/MWh, driven by rapidly escalating structural cost and only marginal improvements in energy capture. This confirms that pushing the rated speed too high yields diminishing returns and is economically unfavorable.

4.6.3 Observation

The sensitivity analysis performed across different rated wind speeds provides an initial indication of how structural and techno-economic performance vary under Mediterranean operating conditions. However, the results obtained through full optimization at each wind speed must be interpreted with caution.
In this study, the Particle Swarm Optimization (PSO) algorithm is independently applied at each rated wind speed, generating structurally and geometrically different blade designs. While this approach allows exploration of the design space, it also introduces a significant level of variability in the results. Therefore, the observed trends in cost and LCOE are affected by the stochastic nature of the optimization process, leading to a dispersion that does not fully reflect a consistent physical relationship between wind speed and cost.

In particular, the resulting cost–wind speed trend does not follow the expected smooth behavior (e.g., linear or quadratic) but instead shows irregular variations since each optimized blade corresponds to a different design configuration. Therefore, the identification of a single optimal rated wind speed based solely on these results may be misleading.

For this reason, the previously obtained graph (Figure 47) is not considered sufficiently robust for a direct techno-economic interpretation within the scope of this thesis. To address this limitation, a simplified and more consistent approach is adopted in the following analysis. Instead of performing a full optimization at each wind speed, a single reference blade, optimized at 10 m/s, is used as a baseline configuration. The effect of varying wind speed is then modeled by scaling the structural thickness through predefined scaling laws. This approach reduces variability, ensures comparability between cases, and allows a more reliable evaluation of the techno-economic trends.

5 Techno-economic analysis

5.1 Introduction

The techno-economic analysis is used to evaluate the LCOE or COE value. The LCOE, i.e. levelized cost of energy, represents the minimum price at which the energy produced by the plant must be sold in order to cover all costs incurred throughout its entire life cycle. Technically, is the revenue required to achieve a rate of return of investment equal to the discount rate over the entire lifetime of the wind farm.
The LCOE is used to compare the cost of electricity production with different technologies. The unit of energy is in €/MWh, so lower is this value, lower will be the cost or higher will be the power product, so better will be the technology analyzed.

$$LCOE = \frac{\sum_{t=1}^{n} \frac{I_t + M_t}{(1+r)^t}}{\sum_{t=1}^{n} \frac{E_t}{(1+r)^t}}$$

Where:
I_t Investment expenditure in year t
M_tOperation, maintenance and service expenditure in year t
E_t Energy generation in year t
r Discount rate or WACC
n Lifetime of the project in years

Today the LCOE of wind technologies is decreasing reaching around 80 €/MWh for the best solution of the wind offshore, still higher of the onshore wind technologies [12].
In this thesis, the techno-economic analysis, for simplicity, is based on the Cost of Energy rather than the Levelized Cost of Energy. The COE simply neglects the discount effect, inflation and so provides a direct relationship between total costs and energy production. The following comparison is strictly related to energy production, and total wind farm costs for each site.

5.2 Base-model for the techno-economic analysis

After completing the optimization procedures described in the previous chapter, the analysis is extended through a dedicated study aimed at identifying a direct relationship between blade structural cost and wind speed. At this stage, the objective is no longer to further optimize the blade geometry or structural layout, but rather to

quantify how the blade cost evolves as increasing wind velocities require progressively higher structural robustness.
The blade optimized, in the precious chapter, at rated wind speed of 10 m/s is selected as a reference configuration. Starting from this baseline design, blade structural properties are modified through the introduction of a single global thickness multiplier applied uniformly to the main structural components (spar cap, shell laminates, shear webs and foam core thickness). In this way, the original optimization problem involving many design variables is reduced to a limited number of structural components governed by a single scaling parameter.
For each wind speed in the range between 8 and 16 m/s, a sequence of blade configurations is generated, with CoBlade without PSO, by progressively increasing the thickness multiplier. A full structural analysis is performed, and the multiplier is increased until both max stress and max buckling are satisfied, both with a max value of 0.5. The minimum multiplier fulfilling these requirements is then selected as the representative solution for the corresponding wind speed.
This procedure ensures that, for each velocity unnecessary overdesign is avoided, at the same time, the resulting blade configurations remain closely related to the refence geometry. The outcome of this study is a monotonic relationship between wind speed and blade cost (Figure 49). In particular, the progressive increase in wind speed leads to higher aerodynamic and inertial loads, which in turn require thicker structural components to maintain acceptable stress and stability margins. This effect translates into an approximately linear increase in blade cost with respect to the thickness multiplier, as shown in Figure 48.

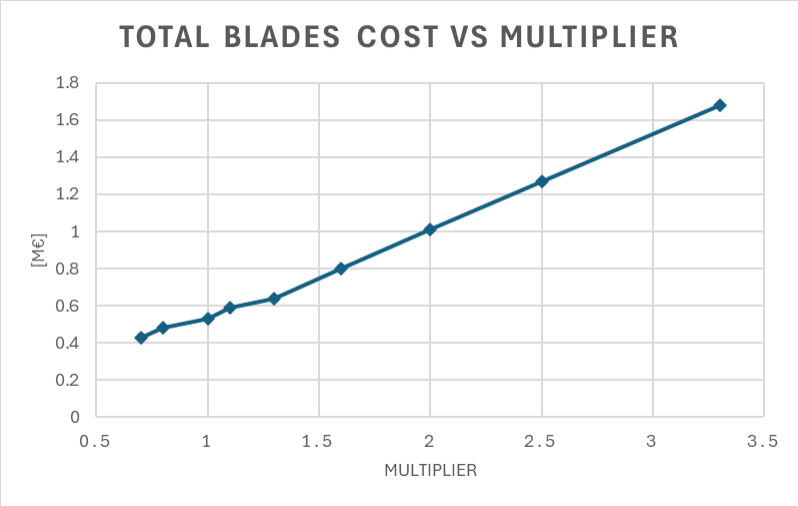

Figure 48: Total blades cost vs multiplier

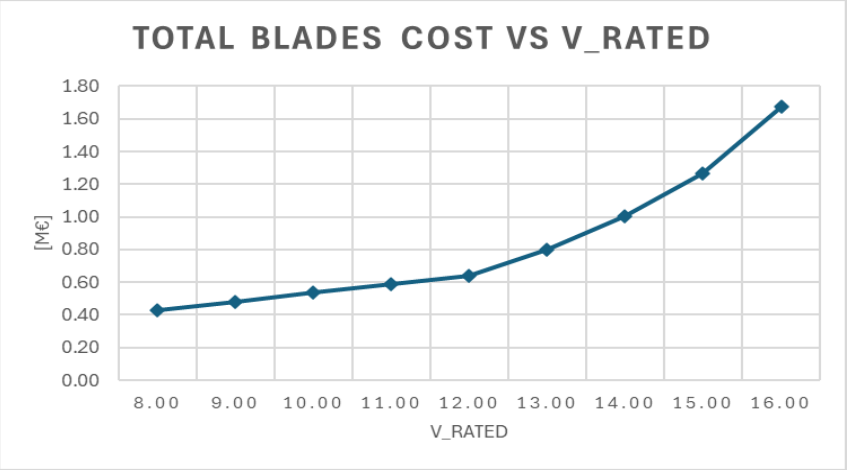

Figure 49: Total blades cost vs v_rated

The present approach enables a transparent and approximate assessment of how increasing wind speeds impact blade cost and so introduces a key point for the following techno-economic analysis.

5.3 Techno-economic comparison across wind speeds and locations

Once the structural sizing strategy was defined and the blade behavior across wind speeds was characterized, the analysis was extended to a techno-economic level in order to understand how these structural trends translate into the cost of energy.

In this phase, the focus was no longer on optimizing the blade geometry, but on evaluating the economic consequences of operating the same optimized turbine design at different wind speeds and in different offshore locations and so aimed at identifying the most suitable location for the installation of a wind farm.

Initially it was considered a large wind farm, made of 60 turbines.

This analysis was done for three different locations: Mar Mediterranean, North Sea and Atlantic Ocean (coast of Canada).

The starting data taken from MATLAB are only the Power and the blade mass. To obtain the COE (Cost Of Energy) is also used the data available in **Error! Reference source not found.**, whit the following assumption:

- A = Development and project management constant whit the turbine power [€]
- B = Wind turbine cost and balance of plant cost directly proportional to the power [€/MW]
- C = Installation and commissioning cost, Operation maintenance and service and Decommissioning cost proportional to the square root of the power [$€/\sqrt{MW}$].

Table 4: Wind farm cost [12]

Category	Rounded cost	Unit
Development and project management	155.000	£/MW
Development and consenting services	72.000	£/MW
Environmental surveys	9.000	£/MW
Resource and metocean assessment	7.000	£/MW
Structure	4.000	£/MW
Sensors	3.000	£/MW
Maintenance	1.000	£/MW
Geological and hydrographical surveys	9.000	£/MW
Engineering and consultancy	9.000	£/MW
Project management	48.000	£/MW
Wind turbine	1.350.000	£/MW
Nacelle	834.000	£/MW
Rotor	360.000	£/MW
Tower	156.000	£/MW
Balance of plant	2.418.000	£/MW
Dynamic array cable	115.000	£/MW
Export cable	269.000	£/MW
Cable accessories	80.000	£/MW
Floating substructure	1.313.000	£/MW
Mooring systems	316.000	£/MW
Offshore substation	282.000	£/MW
Onshore substation	44.000	£/MW
Installation and commissioning	1.376.000	£/MW
Inbound transport	154.000	£/MW
Mooring and anchoring pre-installation	153.000	£/MW
Floating substructure - turbine assembly	72.000	£/MW
Floating substructure - turbine installation	114.000	£/MW
Offshore cable installation	171.000	£/MW
Onshore export cable installation	8.000	£/MW
Offshore substation installation	52.000	£/MW
Onshore substation construction	29.000	£/MW
Offshore logistics	13.000	£/MW
Sea-based support	6.000	£/MW
Marine coordination	2.000	£/MW
Weather forecasting and metocean data	1.000	£/MW
Marine safety and rescue	4.000	£/MW
Contingency and insurance	610.000	£/MW
Operation. maintenance and service	98.000	£/MW/Year
Operations. maintenance and service port	0	£/MW/Year
Operations	34.000	£/MW/Year
Offshore logistics	7.000	£/MW/Year
Maintenance and service	57.000	£/MW/Year
Decommissioning	450.000	£/MW

In this way the total wind farm cost is obtained from the following equation:

$$C_{tot} = A + B \cdot P + C \cdot \sqrt{P}$$

Follow the Cost of Energy calculation:

$$COE = \frac{C_{tot}}{AEP \cdot n}$$

With 'n' the lifetime of the plant, considered of 25 years, and AEP the annual energy production that is obtain from the Power and the Capacity Factor (CF), that change not only with the velocity but also with the location, increasing going from the lowest in the Mediterranean Sea to the highest in the Atlantic Ocean.

$$AEP = h_{yaer} \cdot P \cdot CF$$

The following curves are obtained:

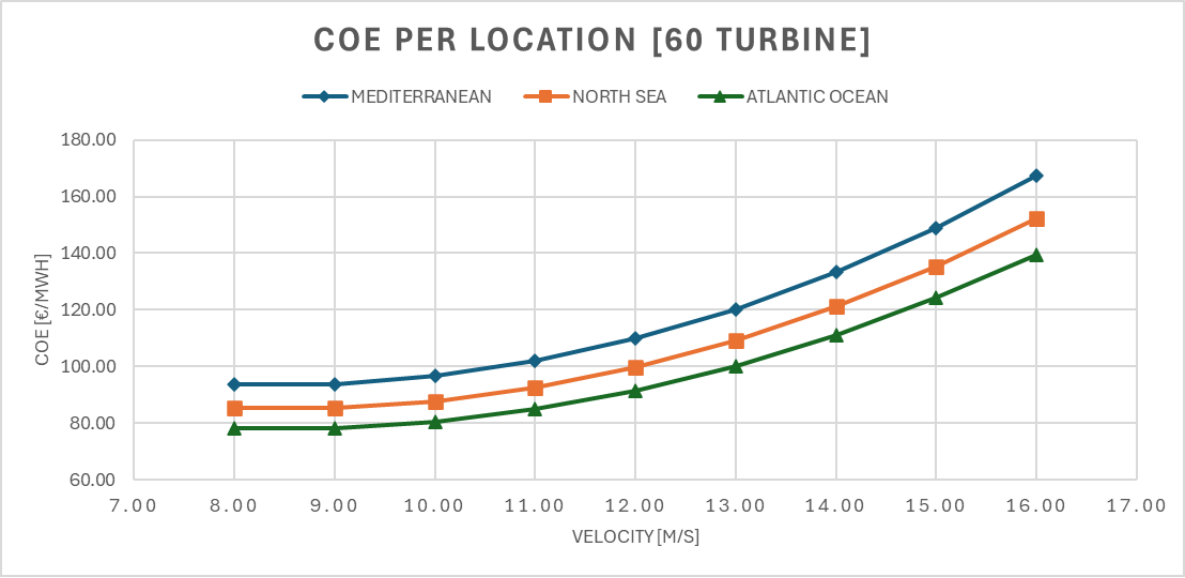

Figure 50: COE for location (60 turbine)

A first observation concerns the absolute COE values. For all wind speeds, the Mediterranean location consistently exhibits the highest COE, while the Atlantic Ocean shows the lowest values, with the North Sea lying in between. This behaviour is primarily driven by differences in capacity factor and annual energy production, which directly influence the denominator of the COE calculation. Despite the same turbine design and cost model being used in all cases, the reduced wind resource availability in the Mediterranean results in a lower AEP and, consequently, higher COE values. Beyond the value the trend is also important because show that for all

three locations, the COE exhibits a shallow minimum at low wind speeds, around 9-10 m/s, followed by a steeper increase as wind speed rises. That's because for higher wind speeds is required significant structural reinforcement (higher multiplier) and so increasing the blade mass and cost. This resulting increase outweighs the benefits of additional energy production beyond a certain wind speed threshold.

Now the same analysis was taken for a plant of 20 turbine instead of 60, reducing so the energy production but also the total cost.

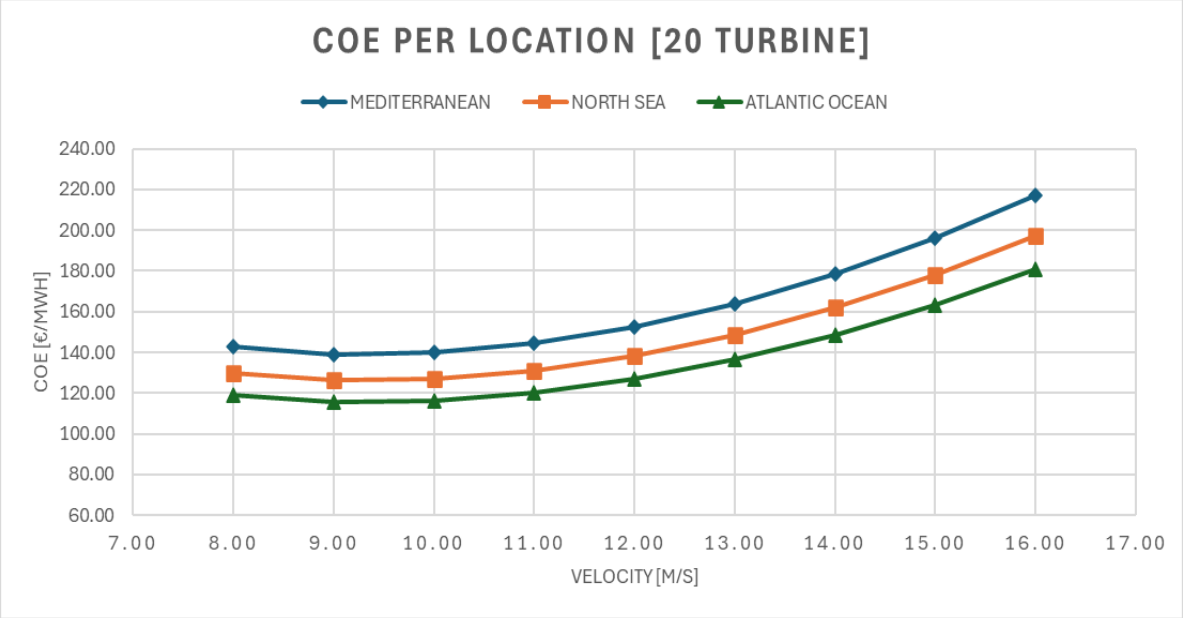

Figure 51: COE for location (20 turbine)

From an absolute perspective, the COE values are systematically higher than those observed for the 60-turbine configuration, regardless of wind speed or location. This behaviour is expected and is primarily attributed to the reduced scale of the wind farm.
This minimum is not coincidental but directly linked to the design methodology adopted in this work. The blade geometry and structural layout were originally optimized at a rated wind speed of 10 m/s. Consequently, the turbine achieves its best compromise between structural cost and energy production in the vicinity of this operating condition. Therefore, the presence of a COE minimum around this wind speed is an expected and physically consistent result.
One important difference whit the 60 turbines case is the spacing between the curves. Compared to the large wind case, the vertical separation between the Mediterranean Sea, North Sea and Atlantic Ocean curves become slightly more pronounced. This indicates that for smaller wind farm, the benefit of operating in high resource locations becomes more significant.

6 Conclusion

This thesis developed and validated an integrated aero-structural and techno-economic framework for the design and assessment of a 15 MW offshore wind turbine blade, with a specific focus on Mediterranean operating conditions. Rather than focusing solely on geometric optimization, the work aimed to investigate how structural sizing, aerodynamic performance, and economic indicators interact under wind regimes characterized by lower average wind speeds.

A primary outcome of this work is the successful generation of a blade design adapted to the Mediterranean context. The structural optimization process demonstrated that it is technically feasible to redesign the blade starting from a North Sea reference configuration, achieving a reduction in the Cost/AEP while maintaining all structural constraints. The frozen-load optimization highlighted the possibility of reducing material usage through an efficient redistribution of laminate thickness, while the subsequent aero-structural optimization further improved performance by coupling structural and aerodynamic variables. The final design exhibited a more uniform strain distribution and a more efficient use of materials, confirming the effectiveness of the proposed framework.

Although a comparative optimization across multiple rated wind speeds was initially performed, these results were not considered sufficiently robust for the final techno-economic assessment. The independent application of the Particle Swarm Optimization at each wind speed leads to structurally and geometrically different blade configurations, increasing the variability of the results and preventing a consistent comparison of cost trends. For this reason, the identification of an optimal rated wind speed based on PSO multi-speed optimization was not retained as a conclusive result within this study.

The techno-economic analysis was therefore conducted using a simplified and more consistent approach, based on a reference blade optimized at 10 m/s and modified through scaling laws applied to structural thickness. This approach allowed the evaluation of the COE trend under varying wind conditions while maintaining comparability between configurations.

The results of the techno-economic analysis indicate that, within the Mediterranean context, the adoption of a specifically optimized blade does not lead to a highly advantageous reduction in the Cost of Energy. This is mainly due to the compensation between structural cost and energy production: lower wind speeds reduce the structural demand and cost, but also significantly decrease the annual energy production. Additionally, the presence of high fixed costs in offshore wind farm deployment limits the overall economic benefit of blade-level optimization alone.

Furthermore, the cost modelling adopted in this work is affected by limitations related to the use of scaling laws, particularly for floating structures, installation, and maintenance costs. These cost components are highly complex and site-dependent, and their representation through simplified scaling relationships requires further validation.

From a structural perspective, the modelling approach could also be improved. The current analysis is based on beam-like structural representations, which, although computationally efficient, may not fully capture local effects. A more advanced finite element modelling approach, such as shell-based models, would allow a more accurate validation of the blade geometry and structural response.

Finally, to strengthen the techno-economic conclusions, further work is required to refine and validate the scaling laws used for cost estimation, as well as to integrate additional effects such as wake interactions within the wind farm.

Overall, this work demonstrates that the design of a blade adapted to Mediterranean conditions is technically feasible, but highlights that its economic advantage is limited and strongly dependent on the accuracy of cost modelling and large-scale system considerations.

Bibliography

[1] Tesup, "Dai mulini a vento all'energia domestica: l'evoluzione delle turbine eoliche," 2023. [Online]. Available: https://tesup.com/it/blogs/post/dai-mulini-a-vento-allenergia-domestica-levoluzione-delle-turbine-eoliche

[2] Wind Energy Science (Copernicus), "Offshore wind energy," vol. 8, 2023. [Online]. Available: https://wes.copernicus.org/articles/8/1873/2023/

[3] Institute for Energy Economics and Financial Analysis (IEEFA), "Cracks in the war wind narrative," 2023. [Online]. Available: https://ieefa.org/resources/ieefa-update-cracks-war-wind

[4] J.-H. Liu, C. J.-C., L. W. J., and S. W.-N., "Extreme load analysis of a 5 MW offshore wind turbine under tropical cyclone wind conditions."

[5] Wind Systems Magazine, "What are transient loads and how do I reduce the effect on my turbines?" [Online]. Available: https://www.windsystemsmag.com/what-are-transient-loads-and-how-do-i-reduce-the-effect-on-my-turbines/

[6] D. C. Sale, *User's Guide to Co-Blade*. Sandia National Laboratories. [Online]. Available: https://github.com/nnmrec/Co-Blade

[7] Pengky, "Aerodynamic of blade," [Online]. Available: https://www.pengky.cn/zz-horizontal-axis-turbine/04-aerodynamic-of-blade/aerodynamic-of-blade.html

[8] Renewable Energy, "Material properties and degradation of wind turbine blades," ScienceDirect, 2023. [Online]. Available: https://www.sciencedirect.com/science/article/pii/S0960148123008728

[9] National Renewable Energy Laboratory (NREL), "Comet wind blade resin technology," [Online]. Available: https://www.nrel.gov/manufacturing/comet-wind-blade-resin

[10] National Renewable Energy Laboratory (NREL), *IEA Wind 15-MW Offshore Reference Turbine*, NREL/TP-5000-75698, 2020. [Online]. Available: https://docs.nrel.gov/docs/fy20osti/75698.pdf

[11] BalticWind.EU, "Onshore and offshore wind: the most cost-competitive power generation globally," 2023. [Online]. Available: https://balticwind.eu

[12] Guide to Floating Offshore Wind, "Wind farm costs," [Online]. Available: https://guidetofloatingoffshorewind.com/wind-farm-costs/

[13] Rinnovabili.it, "Pala eolica riciclabile Siemens Gamesa," [Online]. Available: https://www.rinnovabili.it/energia/eolico/pala-eolica-riciclabile-simens-gamesa/

[14] Rinnovabili.it, “Installate le prime pale eoliche in legno nel mondo,” [Online]. Available: https://www.rinnovabili.it/energia/eolico/installate-prime-pale-eoliche-in-legno-mondo/

[15] Voodin Blade Technology, “Wooden wind turbine blades,” [Online]. Available: https://voodin-blades.com/

[16] DTU Orbit, “Floating offshore wind research report,” Technical University of Denmark. [Online]. Available: https://backend.orbit.dtu.dk/ws/portalfiles/portal/7728949/ris_r_1280.pdf

[17] National Grid, “History of wind energy,” [Online]. Available: https://www.nationalgrid.com/stories/energy-explained/history-wind-energy

[18] Energy Break, “Eolico offshore alla conquista dei mari,” [Online]. Available: https://www.energybreak.it/eolico-offshore-alla-conquista-dei-mari/

[19] ESG360, “Eolico offshore: vento contrario per il progetto europeo,” [Online]. Available: https://www.esg360.it/energia-rinnovabile/eolico-offshore-vento-contrario-per-il-progetto-europeo/

[20] Energia Italia News, “Offshore galleggiante: il futuro dell’eolico in Italia,” [Online]. Available: https://www.energiaitalia.news/news/eolico/offshore-galleggiante-il-futuro-delleolico-in-italia-e-nel-mediterraneo-lo-studio/41295/

[21] PMC, “Wind energy research article,” 2024. [Online]. Available: https://pmc.ncbi.nlm.nih.gov/articles/PMC11269837/

Ringraziamenti

Adesso scrivo probabilmente la parte più difficile della tesi: i ringraziamenti.
Nella mia testa mi chiedo: “dovrei partire in ordine cronologico?”, “dal più importante al meno importante?”, oppure “dal meno importante al più importante?”. In realtà credo che l’ordine abbia poca importanza, perché alla fine voglio ringraziare tutte le persone che, in un modo o nell’altro, mi hanno aiutato a raggiungere questo traguardo.
Da qualcuno però devo pur iniziare, e voglio farlo da due persone in particolare che, in modo diverso rispetto a tutti gli altri, hanno contribuito a farmi arrivare fino a qui. In realtà non mi hanno incoraggiato, anzi. Dicendomi che non ero molto bravo o abbastanza intelligente, che forse non sarei riuscito a raggiungere questo obiettivo e che sarebbe stato meglio cambiare strada, hanno acceso in me qualcosa che mi ha dato la motivazione per dimostrare il contrario.
Quindi grazie, “professoresse”.
Detto questo, vorrei ringraziare tutte quelle persone che invece hanno contribuito in maniera positiva al mio percorso. Parto dal mio coinquilino Federico che, per cinque anni, mi ha aiutato in tutti i modi possibili: dai primi esami fino all’ultimo. Tutto è iniziato da quell’idea che avevamo alle superiori: vivere insieme per studiare di più. Poteva sembrare paradossale, ma posso dire con certezza che ha funzionato, e non mi pento nemmeno per un giorno di aver preso questa decisione.
Parlando di decisioni, ognuno nella propria vita sceglie i propri amici, e io non potevo fare scelta migliore.
Come avrete capito negli anni, non sono molto bravo a mostrare ciò che provo. Ma se oggi scrivo queste righe è perché ognuno di voi occupa un posto importante nella mia vita.
Partendo dal gruppo di Torino: dopo ogni lezione, dopo intere giornate passate a studiare, il mio unico pensiero era passare un po’ di tempo con voi per alleggerire la mente e dimenticare per qualche ora tutto il resto.
Per questo voglio ringraziare Luca Di Raimondo, esempio da seguire fin dal primo anno di superiori; Luca Ragusa, il madrileno con cui ho passato momenti indimenticabili; Giovanni Sparacino, l’amico trovato grazie ad un semplice messaggio: “Hai un posto in macchina per scendere a Marina?”; Mattia Siniscalchi, l’avvocato con cui ogni momento diventa un ricordo incredibile; e Ludovica Zacco, l’amica con cui posso parlare di tutto, sempre.
Senza di voi questa laurea forse non sarebbe arrivata così presto… o forse non sarebbe arrivata affatto.
Uscendo da Torino, ci sono altre persone che voglio ringraziare. Francesca Rappocciolo, l’amica con lo stesso destino di essere odiati dai professori; Graziana

La Ferla, la mia compagna di quad sull'Etna con cui ho rischiato la vita; Roberta Garaffa, con le lunghe videochiamate che riescono sempre a migliorare la giornata; e infine Andrea La Ferla. Dopo le partitelle al campetto da piccoli ci siamo ritrovati anni dopo, e da quel momento in poi ti ringrazio per la tua presenza costante nella mia vita.
Grazie davvero a tutti voi. Vi voglio bene.
Un ringraziamento speciale va poi al mio coinquilino dai 0 ai 24 anni: mio fratello Marco. Nonostante le continue discussioni, sei sempre stato una guida per me. Ogni volta che avevo un dubbio, di qualsiasi tipo, eri sempre pronto ad aiutarmi. Non potrei esserti più grato. Abbiamo condiviso la stessa stanza per 24 anni, e anche se adesso ognuno prenderà la propria strada e avrà nuovi coinquilini o amici, nessuno potrà mai essere un coinquilino alla tua altezza.
Grazie alla mia famiglia, in particolare ai miei nonni e alle chiamate quotidiane di nonna che mi fanno sentire sempre a casa.
Infine, vorrei dedicare questa laurea e tutto il mio percorso a mamma e papà.
Grazie mamma per esserci sempre stata ed aver creduto sempre in me, la tua incredibile forza è sempre stata, e sempre sarà una fonte di ispirazione.
Grazie papà, per non aver mai dubitato di me e soprattutto per un tuo consiglio che mi desti molti anni fa, che probabilmente non ricorderai neanche: "cammina sempre a testa alta". Non so perché ma quel momento mi è rimasto impresso, e seguo questo consiglio in ogni cosa che faccio.
Quindi grazie mamma e papà, siete miei genitori, a cui devo tutto. So quanti sacrifici avete fatto per permettermi di arrivare fino a qui e non mi avete mai fatto mancare nulla. Voglio solo dirvi che da ora in poi cercherò di ripagarvi, almeno in parte, per tutto quello che mi avete dato.
Vi voglio tanto bene.
Vorrei concludere citando una frase di una canzone che ho seguito fedelmente durante tutto il mio percorso:

"L'ansia ti frega, chi vuoi che creda
Se anche tu non credi in te
Però ricorda che chi sopporta
Tutto il sudore e lo stress
Arriva al top"

Grazie a tutti.